LITHOS 456–457 (2023) 107330

Contents lists available at ScienceDirect

LITHOS

journal homepage: www.elsevier.com/locate/lithos

Large-volume Permian felsic volcanism in the Tisza Mega-unit (East-Central Europe): Evidence from mineralogy, petrology, geochemistry, and geochronology

Máté Szemerédi [a,b,*,1], Andrea Varga [b,1], Réka Lukács [a,c], István Dunkl [d], Ioan Seghedi [e], Mihai Tatu [e,†], Zoltán Kovács [a,f], Béla Raucsik [b], Zsolt Benkó [g,h], Szabolcs Harangi [a,i], Elemér Pál-Molnár [a,b]

[a] MTA-ELTE Volcanology Research Group, Eötvös Loránd Research Network (ELKH), Pázmány Péter sétány 1/C, H-1117 Budapest, Hungary
[b] Department of Mineralogy, Geochemistry and Petrology, 'Vulcano' Petrology and Geochemistry Research Group, University of Szeged, Egyetem st. 2, H-6722 Szeged, Hungary
[c] Institute for Geological and Geochemical Research, Research Centre for Astronomy and Earth Sciences (MTA Centre of Excellence), Eötvös Loránd Research Network (ELKH), Budaörsi út 45, H-1112 Budapest, Hungary
[d] Geoscience Center, Department of Sedimentology & Environmental Geology, University of Göttingen, Goldschmidtstr. 3, D-37077 Göttingen, Germany
[e] Institute of Geodynamics "Sabba S. Ştefănescu", Romanian Academy, 19-23 Jean-Luis Calderon St., Bucharest-37, Romania
[f] Centre for Energy Research, Eötvös Loránd Research Network (ELKH), Konkoly-Thege Miklós út 29-33, H-1121 Budapest, Hungary
[g] Department of Mineralogy and Geology, University of Debrecen, Egyetem tér 1, H-4032 Debrecen, Hungary
[h] Isotope Climatology and Environmental Research Centre (ICER), Institute of Nuclear Research, Hungarian Academy of Sciences, Bem tér 18/C, H-4026 Debrecen, Hungary
[i] Department of Petrology and Geochemistry, Institute of Geography and Earth Sciences, Eötvös Loránd University, Pázmány Péter sétány 1/C, H-1117 Budapest, Hungary

ARTICLE INFO

Keywords:
Permian
Carpathian–Pannonian region
Felsic volcanism
Petrology
Geochronology
Postmagmatic alterations

ABSTRACT

Permian felsic volcanic rocks are widespread in the Tisza Mega-unit (Carpathian–Pannonian region), covering a relatively large area from southern Transdanubia (Hungary) to the Apuseni Mountains (Romania). The present occurrence and structural position of these Permian volcanic rocks are the result of a complex tectonic evolution (including Alpine nappe stacking and Neogene extension); meanwhile, multiple hydrothermal effects and deformation modified their microtexture and chemical composition. In this study, the same emphasis was given to Permian felsic volcanism as well as the subsequent fluid- and/or deformation-related processes in the Tisza Mega-unit to extend our knowledge in regional issues (e.g., geochronology, stratigraphy, and lithologic correlations) and to investigate if the variably altered volcanic rocks can be used in petrogenetic studies.

The zircon U-Pb dating yields ages of ~270.4–262.9 Ma for the Apuseni samples and ~268.4–260.2 Ma for those of the Pannonian Basin. Whole-rock geochemistry, considering immobile trace elements, since most of the major element compositions were severely modified by alteration processes, indicates that the studied rocks are dacite to rhyolite. They belong to a voluminous silicic volcanism during the Middle Permian, most probably related to rifts.

Petrography, whole-rock geochemistry, and X-ray powder diffraction mineralogy revealed that the predominant alteration of the studied rocks is hydrothermal sericitization, locally superimposed by mylonitization in greenschist to subgreenschist conditions during Alpine orogeny. The K-Ar dating of the separated illite fractions confirms that the ductile deformation acted during the Turonian nappe stacking, as the main Alpine deformation phase in the study area.

* Corresponding author at: MTA-ELTE Volcanology Research Group, Eötvös Loránd Research Network (ELKH), Pázmány Péter sétány 1/C, H-1117 Budapest, Hungary.

E-mail addresses: szemeredi.mate@gmail.com (M. Szemerédi), raucsikvarga@geo.u-szeged.hu (A. Varga), reka.harangi@gmail.com (R. Lukács), istvan.dunkl@geo.uni-goettingen.de (I. Dunkl), seghedi@geodin.ro (I. Seghedi), mtatu@geodin.ro (M. Tatu), kozraat@gmail.com (Z. Kovács), raucsik@geo.u-szeged.hu (B. Raucsik), benko.zsolt@science.unideb.hu (Z. Benkó), szabolcsharangi@gmail.com (S. Harangi), palm@geo.u-szeged.hu (E. Pál-Molnár).

[1] The first two authors have contributed equally to this work.

[†] Deceased.

https://doi.org/10.1016/j.lithos.2023.107330
Received 2 May 2023; Received in revised form 11 August 2023; Accepted 12 August 2023
Available online 15 August 2023

On a regional scale, the Permian magmatism in the Tisza Mega-unit looks significantly younger than the similar magmatic activity of the stable Europe (~300–290 Ma).

1. Introduction

In the Carpathian–Pannonian region, the products of several Late Paleozoic magmatic episodes can be seen in outcrops (e.g., Apuseni Mts, southern Transdanubia, Western Carpathians; Vozárová et al., 2009a, 2009b; Nicolae et al., 2014; Bonin and Tatu, 2016; Ondrejka et al., 2022; Szemerédi et al., 2020a, 2021; Villaseñor et al., 2021) or in drillings of the basement of the Pannonian Basin (Szemerédi et al., 2020a, 2020b). Petrological and geochronological studies revealed that the Permian magmatism of the region was associated with a post-collisional to extensional setting (continental rifting) along the northern shore of the Paleo-Tethys (see, e.g., Stampfli and Kozur, 2006), and possibly lasted from the latest Carboniferous–earliest Permian to the earliest Triassic with several distinct episodes (Szemerédi et al., 2021 and references therein).

Among these episodes, based on the silicic volcanic rocks in the Pannonian Basin and the Highiş granitoids in the SW Apuseni Mts (Fig. 1), the Permian magmatism of the Tisza Mega-unit (Tisza MU) proved to be one of the youngest in East-Central Europe (~268–260 Ma; Szemerédi et al., 2020a, 2021), showing an anorogenic (A-type) character. Despite the detailed study of the Permian felsic volcanic rocks in the Pannonian Basin (Szemerédi et al., 2020a), similar formations of the Apuseni Mts (Bleahu et al., 1981; Nicolae et al., 2014; Seghedi et al., 2001) have not been dated so far or compared to the former ones on a petrological and geochronological basis. The latter comparison together with the extension of the available information about the Permian magmatism in the Tisza MU could bear a great potential to explore local to regional correlations, as well as to gain fundamental knowledge in the lithostratigraphy. Furthermore, reconstruction of a large-scale, voluminous, ancient magmatic system with feasible plutonic–volcanic connections (Szemerédi et al., 2021) and bimodal activity (Bonin and Tatu, 2016; Nicolae et al., 2014) could provide valuable information for understanding the more recent ones. As various postmagmatic alterations affected some of these volcanic rocks (e.g., Alpine deformation and/or low-grade metamorphism, K-metasomatism, hydrothermal alteration; Ciobanu et al., 2006; Nicolae et al., 2014; Bonin and Tatu, 2016; Szemerédi et al., 2020a), their compositions should be treated cautiously; however, these alterations could provide an excellent possibility to test the reliability of geochemical and geochronological data for altered Paleozoic volcanic rocks.

Consequently, the following goals were established in this investigation: (1) petrographic, bulk geochemical, and zircon U-Pb geochronological characterization of the Permian felsic volcanic rocks of the Apuseni Mts; (2) extension of the geochemical and geochronological database of the Permian volcanic rocks in the Tisza MU from the basement of the Pannonian Basin; (3) interpretation of the petrological and geochronological results, including felsic rocks in the Pannonian Basin and Permian granitoids in the Apuseni Mts (Szemerédi et al., 2020a, 2020b, 2021); (4) examination of the effects of the postmagmatic alterations on petrographic and geochemical compositions as well as the zircon ages, and (5) obtain new local to regional correlations of the Permian lithostratigraphic units.

2. Geological background

The Tisza MU forms the basement of the Pannonian Basin south of the Mid-Hungarian line (Fig. 1a). Its pre-Neogene basement formations occur on the surface in various areas of the Carpathian–Pannonian region (e.g., Apuseni Mts, Mecsek Mts, Villány Mts, and Slavonian Mts), among which Permian felsic volcanic rocks occur in the western–central part of the Apuseni Mts (Nicolae et al., 2014) and in the western Mecsek Mts (Szemerédi et al., 2020a). However, Upper Paleozoic basement rocks were penetrated by numerous uranium ore (southern Transdanubia; Barabásné Stuhl, 1988) and hydrocarbon (eastern Pannonian Basin; Kőrössy, 2005) exploration works during the second half of the 20th century, leading to pointwise information about the Permian magmatism in the currently covered part of the Tisza MU (Szemerédi et al., 2020a, 2020b).

Previous petrographic, bulk geochemical, and zircon U-Pb geochronological analyses of the Permian silicic volcanic rocks from southern Transdanubia (western Mecsek Mts, northern foreland of the Villány Mts, and Máriakéménd–Báta area) as well as the eastern Pannonian Basin (Battonya–Pusztaföldvár Basement Ridge and Kelebia area) revealed that all the studied materials (Fig. 1a) belong to a relatively short-lived, Middle Permian (~267–260 Ma), voluminous, rhyodacitic/dacitic to rhyolitic, rift-related volcanism dominated by explosive Plinian eruptions (Szemerédi et al., 2020a, 2020b). Based on their striking whole-rock geochemical similarities with the Permian felsic pyroclastic rocks occurring in the Apuseni Mts (Codru-Moma and Bihor Mts, Fig. 1b and d; Nicolae et al., 2014), a strong correlation was suggested (without direct geochronological evidence; Szemerédi et al., 2020a). Furthermore, based on the detailed petrological and geochronological study of the A-type granitoids of the Middle Permian (~268–263 Ma; Pană et al., 2002; Szemerédi et al., 2021) Highiş igneous complex (Highiş Mts, SW Apuseni Mts; Tatu, 1998; Bonin and Tatu, 2016), possible Permian plutonic–volcanic connections were raised within the Tisza MU (Szemerédi et al., 2021).

The present-day structure of the Apuseni Mts (Fig. 1b) reflects the results of multiple Alpine tectonic events (Ionescu and Hoeck, 2010). It comprises four distinct tectonic units from bottom to top: (1) the Bihor Autochtone Unit (Bihor AU), (2) the Codru Nappe System (Codru NS), (3) the Biharia Nappe System (Biharia NS), and (4) the Mureş zone unit (Balintoni, 1997; Balintoni et al., 2009; Bleahu et al., 1981; Schmid et al., 2008). Although the Bihor AU and the Codru NS unequivocally represent the Tisza MU, the area of the Biharia NS is a matter of debate. Some studies (see, e.g., Csontos and Vörös, 2004), traditionally, suggest that the Biharia NS belongs to the Tisza MU; however, recent tectonostratigraphic works place it in the Dacia Mega-unit (Dacia MU; e.g., Schmid et al., 2008, 2020; Kounov and Schmid, 2013). The most important arguments for attributing the Biharia NS to the Dacia MU are based on the timing of nappe stacking and the direction of tectonic transport. Additionally, the Biharia NS was affected by ophiolite obduction, as other parts of the Dacia MU (Schmid et al., 2008, 2020).

Permian volcanic rocks in the Apuseni Mts are relatively abundant in the Codru NS, less prevalent in the Biharia NS, and sporadic in the Bihor AU (Nicolae et al., 2014; Fig. 1b). In the Codru NS, felsic volcanic rocks occur in several localities (structurally representing the Finiş, the Dieva, and the Moma Nappes; Fig. 1d). In the area of the Dieva and Moma Nappes, silicic rocks are associated with basaltic to andesitic lavas as a result of bimodal volcanism (Nicolae et al., 2014). In the Biharia NS, Permian felsic rocks occur in the Arieşeni, the Gârda (Fig. 1d), and the Highiş–Muncel Nappes (Fig. 1b). The latter formations in the Biharia NS were often affected by strong Alpine deformation and/or overprinting by hydrothermal fluids, as well as by low-grade metamorphism because the area is cut across by a greenschist facies shear zone, the Highiş–Biharia Shear Zone (HBSZ, Pană and Erdmer, 1994; Pană et al., 2002; Fig. 1a and b).

The basement of the Tisza MU in Hungary is also subdivided into three main Alpine facies zones, the socalled Mecsek, Villány (also referred as Villány–Bihor), and Békés (also referred as Békés–Codru)

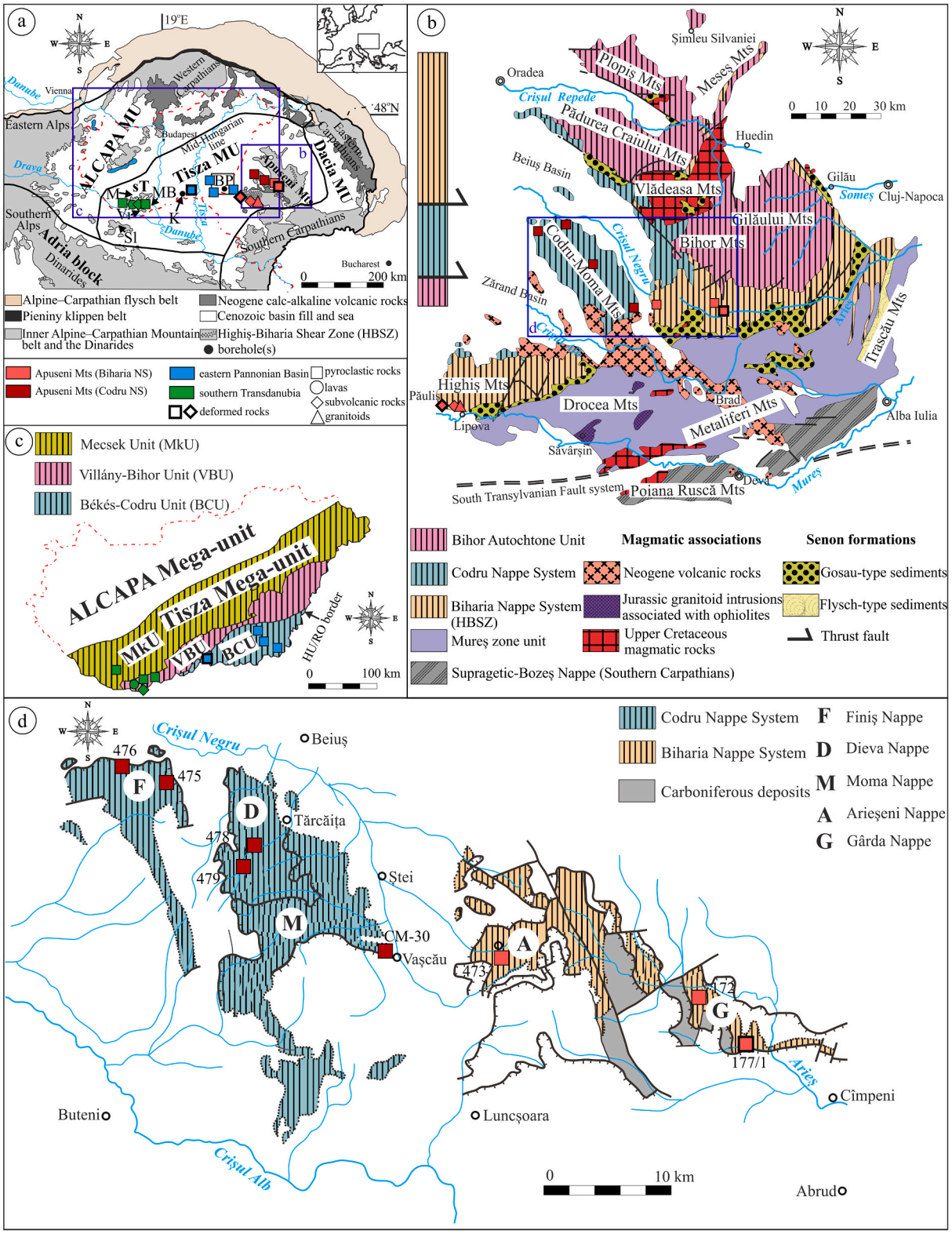

Fig. 1. (a) Tectonic sketch of the Carpathian–Pannonian region pointing out the occurrences of the Permian magmatic formations in the Tisza Mega-unit (simplified after Csontos and Vörös, 2004; Szemerédi et al., 2020a); (b) Simplified geological map of the Apuseni Mts showing its Alpine nappe systems (see column), the most significant rock associations, and the localities of the studied Permian felsic volcanic rocks (modified after Balintoni et al., 2009; Ionescu and Hoeck, 2010); (c) Mesozoic facies zones in the basement of the Tisza Mega-unit (Hungary, modified after Szederkényi et al., 2013); (d) Occurrences of the studied Permian felsic volcanic rocks in the Codru-Moma and Bihor Mts (western–central Apuseni Mts; modified after Nicolae et al., 2014). Abbreviations: *BP* Battonya–Pusztaföldvár Basement Ridge, *K* Kelebia area, *M* Mecsek Mts, *MB* Máriakéménd–Báta area, *Sl* Slavonian Mts, *sT* southern Transdanubia, *Vi* Villány Mts.

Units (from north to south; Fig. 1c). According to the traditional approach, the Villány and Békés Units correlate with the Bihor AU and the Codru NS, respectively, while the Mecsek Unit and the Biharia NS do not have Alpine correspondence (Szederkényi et al., 2013).

3. Materials and methods

The studied samples (Table 1) derive from three distinct regions of the Tisza MU (Apuseni Mts, eastern Pannonian Basin, and southern Transdanubia; Fig. 1). Most of the materials were collected in the western–central part of the Apuseni Mts, representing 9 localities. These samples include felsic pyroclastic rocks from the Codru-Moma Mts and slightly altered to low-grade metamorphic pyroclastites from the Bihor Mts according to Nicolae et al. (2014); and deformed subvolcanic rocks from the Highiş Mts. As some of the relatively pristine, silicic volcanic rocks of the Codru-Moma and Bihor Mts were previously described and interpreted (Nicolae et al., 2014), we have also focused on the less explored, altered (e.g., strongly deformed, hydrothermally overprinted, or metamorphosed) varieties, collected in the HBSZ.

To gain additional age constraints on the Permian felsic volcanism in the Tisza MU, several drill cores were selected for zircon U-Pb dating and geochemical analyses from the eastern Pannonian Basin and southern Transdanubia (Table 1). In total, 5 samples were involved from the Battonya–Pusztaföldvár Basement Ridge (Battonya, Nagyszénás, and Tótkomlós areas) and another one from the Kelebia area. A single sample represents the Máriakéménd–Báta area (Fig. 1a). Furthermore, the chemistry of garnet crystals in crystal-rich pyroclastic rocks was analyzed from the Codru-Moma Mts as well as the northern foreland of the Villány Mts, southern Transdanubia (boreholes Egerág–7 and Szalánta–3).

Petrographic studies, including mineralogical and textural observations, were done at the Department of Mineralogy, Geochemistry and

Table 1
The most relevant information about the studied materials, including sampling details and the results of the petrographic and geochemical classification (previous results published in Szemerédi et al., 2020a are in italics; samples lacking whole-rock geochemical data are marked by asterisk).

Sample	Region	Area (tectonic unit/nappe system, nappe)	Locality	GPS coordinates	Rock type	Geochemical classification (trace elements)
172	Apuseni Mts	Bihor Mts (Biharia NS, Gârda N)	Huzinesti Valley	N46.401444 E22.917250	pyroclastic (ignimbrite)	rhyodacite/dacite
177/1	Apuseni Mts	Bihor Mts (Biharia NS, Gârda N)	Valea Vadului	N46.435917 E22.850597	pyroclastic (deformed ignimbrite)	rhyodacite/dacite
473	Apuseni Mts	Bihor Mts (Biharia NS, Arieşeni N)	Băiţa Plai	N46.485833 E22.617886	pyroclastic (ignimbrite)	rhyodacite/dacite
475	Apuseni Mts	Codru-Moma Mts (Codru NS, Finiş N)	Zărşag Valley	N46.618053 E22.151186	pyroclastic (ignimbrite)	rhyodacite/dacite
476	Apuseni Mts	Codru-Moma Mts (Codru NS, Finiş N)	Botfei Valley	N46.585667 E22.150356	pyroclastic (ignimbrite)	rhyodacite/dacite
478	Apuseni Mts	Codru-Moma Mts (Codru NS, Dieva N)	Tărcăiţa Valley	N46.552181 E22.268753	pyroclastic (ignimbrite)	rhyodacite/dacite
479	Apuseni Mts	Codru-Moma Mts (Codru NS, Dieva N)	Tărcăiţa Valley	N46.560556 E22.271250	pyroclastic (ignimbrite)	rhyodacite/dacite
CM-30	Apuseni Mts	Codru-Moma Mts (Codru NS, Moma N)	Vaşcău	N46.47837 E22.47189	pyroclastic (ignimbrite)	rhyodacite/dacite
OPR1–5	Apuseni Mts	Highiş Mts (Biharia NS, Highiş-Muncel N)	Păuliş (5 samples, OPR1–5)	N46.1233283 E21.6119117	subvolcanic (variously deformed microgranite)	rhyolite
Bat–18*	eastern Pannonian Basin	Battonya–Pusztaföldvár BR (BCU)	Battonya–18 borehole	N46.289797 E21.021296	pyroclastic (ignimbrite)	
Bat-E*	eastern Pannonian Basin	Battonya–Pusztaföldvár BR (BCU)	Battonya area (5 boreholes)		pyroclastic (ignimbrite)	
Bat-M*	eastern Pannonian Basin	Battonya–Pusztaföldvár BR (BCU)	Battonya area (9 boreholes)		pyroclastic (rheoignimbrite)	
*BATR/1**	*eastern Pannonian Basin*	*Battonya–Pusztaföldvár BR (BCU)*	*Tótkomlós-K–3 borehole*	*N46.408374 E20.867368*	*volcaniclastic*	
BATR/2	*eastern Pannonian Basin*	*Battonya–Pusztaföldvár BR (BCU)*	*Tótkomlós-K–3 borehole*	*N46.408374 E20.867368*	*volcaniclastic*	*rhyodacite/dacite*
Nsz–2*	eastern Pannonian Basin	Battonya–Pusztaföldvár BR (BCU, tectonized area)	Nagyszénás–2 borehole	N46.684436 E20.646740	pyroclastic (ignimbrite)	
T–I	eastern Pannonian Basin	Battonya–Pusztaföldvár BR (BCU, tectonized area)	Tótkomlós–I borehole	N46.446599 E20.755479	pyroclastic (lava-like ash tuff)	rhyolite
Kel–7	*eastern Pannonian Basin*	*Kelebia area (BCU)*	*Kelebia–7 borehole*	*N46.176431 E19.636259*	*pyroclastic (deformed ignimbrite)*	*rhyodacite/dacite*
Kel–11*	eastern Pannonian Basin	Kelebia area (BCU)	Kelebia–11 borehole	N46.170843 E19.626279	pyroclastic (deformed ignimbrite)	
Bt–3	southern Transdanubia	Máriakéménd–Báta area (VBU)	Báta–3 borehole	N46.128202 E18.767379	pyroclastic (ignimbrite)	rhyodacite/dacite
Gy–1	*southern Transdanubia*	*western Mecsek Mts (MkU)*	*Gyűrűfű*	*N46.109800 E17.934017*	*pyroclastic (ignimbrite)*	*rhyodacite/dacite*
Sz–1	*southern Transdanubia*	*northern foreland of the Villány Mts (VBU)*	*Szava–1 borehole*	*N45.895575 E18.185042*	*lava*	*rhyodacite/dacite*
Szl–3	*southern Transdanubia*	*northern foreland of the Villány Mts (VBU)*	*Szalánta–3 borehole*	*N45.974080 E18.230271*	*pyroclastic (ignimbrite)*	*rhyodacite/dacite*
Eá–7	*southern Transdanubia*	*northern foreland of the Villány Mts (VBU)*	*Egerág–7 borehole*	*N45.960195 E18.305899*	*pyroclastic (ignimbrite)*	*rhyodacite/dacite*
Eá–7d	southern Transdanubia	northern foreland of the Villány Mts (VBU)	Egerág–7 borehole	N45.960195 E18.305899	dyke	rhyodacite/dacite

Bat-E and Bat-M samples were compiled of small pieces of drill core materials from 5 and 9 adjacent boreholes of the Battonya area (eastern Pannonian Basin), representing eutaxitic, massive, matrix-supported, porphyritic, fiamme-bearing lappili tuffs and felsitic, matrix-supported, porphyritic, fiamme-bearing rheomorphic lapilli tuffs, respectively (see details in Szemerédi et al., 2020b). Abbreviations: *BR* basement ridge, *N* nappe, *NS* nappe system, *BCU* Békés–Codru Unit, *MkU* Mecsek Unit, *VBU* Villány–Bihor Unit.

Petrology, University of Szeged, on thin sections. Modal compositions (vol%) were measured by point counting (at least 500 points per thin section) in 21 selected representative samples using the JMicroVision software (Roduit, 2019). The microstructural analysis of the deformed and/or metamorphosed samples was based on Blenkinsop (2000) and Passchier and Trouw (2005) using oriented thin sections. Some accessory and opaque minerals were identified by a Thermo Scientific DXR Raman spectrometer. Measurements were performed using a x50 objective lens, 25–50 μm pinhole aperture, and a 780 nm Nd-YAG laser with an irradiation power between 1 and 12 mW. Petrographic descriptions were also supplemented by semiquantitative analyses using an AMRAY 1830 scanning electron microscope (SEM) equipped with an EDAX PV 9800 energy-dispersive spectrometer at the Department of Petrology and Geochemistry of Eötvös Loránd University, Budapest, under the following conditions: 20 kV accelerating voltage, 1 nA beam current, and 100 s acquisition time.

Detailed mineralogical analysis was performed on the pervasively foliated sample 177/1 (Biharia NS) to characterize postmagmatic alterations using X-ray powder diffraction (XRPD) techniques at the Department of Mineralogy, Geochemistry and Petrology, University of Szeged. Additionally, the separated size fractions of illite (sample 177/1) were analyzed using the unspiked K-Ar method (see detailed in the Appendix), following the procedure laid out by Matsumoto and Kobayashi (1995) at the Geochronology Laboratory of the Institute for Nuclear Research, Debrecen, Hungary.

Bulk-rock geochemical analyses were performed at the Bureau Veritas Mineral Laboratories (AcmeLabs, Vancouver, Canada) using ICP-ES and ICP-MS methods. The analytical conditions were the same as those of Szemerédi et al. (2020a).

The compositions of garnet crystals were analyzed at the Department of Geochemistry, Georg-August University, Göttingen, Germany using a JEOL JXA 8900 RL electron microprobe. The analytical conditions of the analyses are summarized in Supplementary Table 1.

U-Pb geochronology was performed on 63–250 μm zircon crystals separated from 14 representative samples (Table 1) by standard heavy mineral separation (crushing, sieving, magnetic separation, heavy liquid separation using sodium polytungstate, and hand picking). The samples represent relatively pristine as well as deformed rocks from the Apuseni Mts (7), the eastern Pannonian Basin (6), and southern Transdanubia (1). The in-situ U-Pb analyses were performed at the GÖochron Laboratories, Georg-August University, Göttingen using laser-ablation single-collector sector-field inductively coupled plasma mass spectrometry (LA–SF–ICP–MS). U-Pb dates were calculated with 95% confidence and error propagation (quadratically propagated external errors) has been done according to Horstwood et al. (2016).

A complete description of the methods used for XRPD and geochronological analyses is available in the Appendix.

4. Results

4.1. Petrography

Most of the studied silicic volcanic rocks are crystal-rich, altered fiamme-bearing, variously welded lapilli tuffs, showing well-preserved pyroclastic texture (e.g., samples 172, 478, 479, CM-30, Gy–1, Szl–3, and Eá–7; Table 1, Fig. 2a to d, Supplementary Fig. 1). Massive, nonporous pyroclastic rocks consist of 20–32 vol% poorly sorted, often fragmented phenocrysts (up to 5 mm) and 4–14 vol% cm–mm-sized devitrified fiamme in a fine-grained groundmass (59–66 vol%). Fiamme (Fig. 2c and d) and devitrified glass shards (Fig. 2a and d) in the matrix are generally flattened and deformed, with a well-visible orientation (eutaxitic texture); however, in some samples (samples 177/1, 473, and 475) these components are barely or not identifiable due to the strong recrystallization (see below). Rock-forming phenocrysts are 8–20 vol% subhedral, resorbed, and often fragmented quartz (up to 5 mm); euhedral or subhedral, fragmented, altered feldspar crystals (up to 4.5 mm) dominated by K-feldspar (5–13 vol%), with a small amount of plagioclase (1–5 vol%), as well as euhedral, variously altered biotite (0–2 vol %, up to 1.5 mm), and pyroxene (0–3 vol%, up to 2 mm; e.g., samples 172, 478, and CM-30) replaced by Fe-Ti oxides. Accessory components are most commonly zircon, apatite, monazite, xenotime, and rutile; in addition, in some rocks, rare tourmaline (samples Szl–3 and Eá–7), allanite (Gy–1) or garnet (samples 476, CM-30, Szl–3, and Eá–7) also occurs.

On the thin section scale, several alteration and deformation features were recognized in the studied crystal-rich pyroclastic rocks. Several samples were affected by sericitization, carbonatization, and/or silicification accompanied by pyrite mineralization (Fig. 2e and f, Supplementary Fig. 2). Around the hematitized pyrite or magnetite crystals face-controlled quartz fringes were locally developed (Supplementary Fig. 2c). The microcracks and thin veinlets are mostly filled with secondary muscovite and/or silica. In tectonically deformed samples (e.g., samples 475, 478, 479, Kel–7, and Kel–11), quartz phenocrysts are fragmented and variably deformed, showing undulatory extinction and deformation lamellae in cross-polarized light (Supplementary Figs. 1 and 2). Furthermore, the deformed ignimbrites have moderately developed pressure-solution seams and show significant recrystallization of the matrix (Fig. 2g). Disjunctive foliation is defined by an oriented fine-grained micaceous material (sericite and/or muscovite). As porphyroclasts, quartz and feldspar crystals have fibrous strain shadows subparallel to the well-developed foliation, showing a gradual transition between the fringes and the matrix (Fig. 2h, Supplementary Fig. 2g and h).

In contrast, the pyroclastic rocks of the Battonya–Pusztaföldvár BR (Table 1, Fig. 3a to c) are relatively crystal-poor (8–20 vol%), matrix-supported, fiamme-bearing (10–12 vol%) lapilli tuffs lacking any mafic component. Based on the textural features, eutaxitic (welded, sample Bat-E) and rheomorphic (sample Bat-M) lapilli tuffs as well as lava-like ash tuffs (sample T–I) were distinguished, all of them showing similar felsic mineral assemblages (3–9 vol% quartz, 3–8 vol% K-feldspar, and 0–5 vol% plagioclase) to the aforementioned crystal-rich samples. Locally, crystal-poor ignimbrites also show alteration and deformation features such as sericitization, silicification, carbonatization, and intracrystalline deformation of quartz. In the eastern Pannonian Basin, poorly sorted lithic-rich volcaniclastics (resedimented pyroclastic or volcanogenic sedimentary rocks) also occur (Supplementary Fig. 3a and b).

Felsic lavas and subvolcanic rocks are sporadic in the study area (Table 1, Fig. 3d to f, Supplementary Fig. 3c to h). The studied samples (e.g., samples OPR2, Sz–1, and Eá–7d) are porphyric (having a crystal content of 25–42 vol%), consisting of 7–15 vol% quartz, 10–35 vol% altered feldspar (both K-feldspar and plagioclase), and 0–3 vol% hematitized biotite. Subvolcanic rocks have a porphyric microholocrystalline texture (Fig. 3d to f), while the lavas are dominantly felsitic, rarely relict perlitic, spherulitic, or granophyric textures are apparent. The samples OPR1 to OPR5 from the Highiş Mts show characteristic microtextures of tectonic deformation and fluid-related processes. Weakly developed foliation is indicated by pressure-solution seams and flattened and boudinaged quartz crystals (Supplementary Fig. 3g and h), showing intracrystalline deformation (undulose extinction, deformation lamellae, and subgrain formation), while biotite, epidote, and hematite appear as secondary minerals (Fig. 3f, Supplementary Fig. 3g).

4.2. Major and trace element geochemistry

The major and trace elements were analyzed in the samples from all the occurrences of Permian felsic volcanic rocks in the Tisza MU (Supplementary Tables 2 and 3), corresponding to the traditional subdivision, and compared with the previous whole-rock geochemical data (Szemerédi et al., 2020a). The Highiş granitoids as feasible plutonic equivalents of the studied volcanic rocks (Szemerédi et al., 2021), were also plotted in the same diagrams. The studied rocks are described

together in the following, however, any geochemical differences are emphasized.

The major chemistry of the felsic volcanic rocks displays strongly variable LOI (0.6 to 8.64 wt%, Supplementary Tables 2 and 3); however, pyroclastic rocks from the Apuseni Mts uniformly have a high LOI (>8 wt%, Supplementary Table 2) regardless of being deformed or not. In the total alkali-silica diagram (Fig. 4a), almost all samples fall into the rhyolite field with 69.2–78.2 wt% SiO_2 and variable alkali contents (5.0–9.7 wt%). A single sample from the eastern Pannonian Basin (Kelebia area) is an exception that plots in the trachyte/trachydacite field. As relatively immobile trace elements are less sensitive for secondary processes and provide a more reliable classification of rocks, the data were also plotted on Zr/TiO_2 vs. Nb/Y diagram (Fig. 4b; Winchester and Floyd, 1977), as well. All crystal-rich pyroclastic rocks, lavas, and dykes (regardless of the alteration state) plot in the rhyodacite/dacite field, with subalkaline character (Nb/Y < 0.6). Only some crystal-poor samples from the eastern Pannonian Basin (Battonya–Pusztaföldvár BR) and subvolcanic rocks (e.g., dykes, microgranites, and aplites) from the Highiş Mts were proven to be rhyolites. Two outlier samples from southern Transdanubia (boreholes Máriakéménd–3 and Vókány–2) fall into the trachyandesite field.

Total REE (ΣREE) values lie in a broad range of 110 ppm to 1248 ppm (samples Eá–7d and 473, respectively; Supplementary Tables 2 and 3). Four samples from the Apuseni Mts (samples 172, 473, CM-30, and OPR1) have a higher ΣREE content than 500 ppm; additionally, these samples also have relatively high values of Y (up to 62 ppm), Ce (up to 582 ppm), Zr (up to 296 ppm), and often Th (up to 74 ppm). The chondrite-normalized REE diagrams (Fig. 5a, c, and e) show definite fractionated REE patterns for the studied volcanic rocks (La_N/Yb_N = 3.4–10.1); however, some exceptions should be noted (see below). The samples show enriched light REE (LREE) and near-flat heavy REE (HREE) patterns (La_N/Sm_N = 2.3–4.7; Gd_N/Yb_N = 1.2–1.9) with various deep negative Eu anomalies (Eu/Eu* = 0.0–0.4). Five samples from the Apuseni Mts (samples 172, 177/1, 473, CM-30, and OPR1, Fig. 5a) moderately differ from the others showing remarkably higher enrichment in LREE (La_N/Yb_N = 15.6–44.9; La_N/Sm_N = 3.5–7.8) and less significant Eu anomaly (Eu/Eu* = 0.3–0.7). On the other hand, the two outlier samples from southern Transdanubia (trachyandesites in Fig. 4b) show completely different patterns from the others, showing lower concentrations in all REE (Fig. 5c).

In the primitive mantle-normalized multielement spider diagram (Fig. 5b, d, and f), the samples generally show a strong enrichment in Rb, Th, U, and K, and a slight enrichment in Ba, Nb, Sr, P, and Ti with various deep local negative anomalies. However, the previously mentioned four REE-enriched and the two REE-depleted samples show slightly different concentrations in other trace elements, as well. In addition to LREE, some of the REE-enriched samples from the Apuseni Mts (Fig. 5b) have higher concentrations of Ba, Th, U, and Sr compared to the primitive mantle. On the contrary, the REE-depleted samples from southern Transdanubia (Fig. 5d) proved to have lower concentrations in Ba, Sr, Hf, Zr, Ti, and Y.

Pyroclastic rocks, lavas, and dykes from the Apuseni Mts and southern Transdanubia showed good correspondence with each other, falling into the border of the volcanic arc granite (VAG) and the within plate granite (WPG) fields or close to the triple junction of VAG, WPG, and ORG (ocean ridge granite, Fig. 6). In contrast, all samples from the eastern Pannonian Basin were plotted in the WPG field. Some of the outlier samples differ from the others again; for example, the two REE-depleted volcanic rocks from southern Transdanubia plot basically in the syncollisional granite field, as well as one of the deformed rocks (177/1) or the altered pyroclastic sample (sample 475).

4.3. Garnet chemistry

Garnet crystals were analyzed in the samples from the Codru-Moma Mts and the northern foreland of the Villány Mts (sample 476 and samples Eá–7 and Szl–3, respectively, Table 1), all of which are crystal-rich rhyodacitic/dacitic pyroclastic rocks. The analyzed subhedral or rarely euhedral crystals (in 100–500 μm average size) or smaller fragments (56 analyses in 14 crystals, Supplementary Fig. 4, Supplementary Table 4) were quite homogeneous with respect to their major element composition, zonation was not observed. The inclusions identified in the crystals were monazite, apatite, ilmenite, rutile, and (chloritized) biotite. In all the analyzed garnet crystals, the compositions of almandine and subordinate pyrope are dominant (Fig. 7), while the spessartine and grossular components are insignificant (CaO <1.5 wt%, MnO <4 wt%). Two of the analyzed crystals (sample Eá–7) are exceptions, showing a higher grossular component (CaO = 4–6.5 wt%, Fig. 7a); furthermore, one of them is also enriched in Mn (MnO = 11–12 wt%, Fig. 7b). The average garnet compositions (excluding the outlier crystals) calculated for the studied samples are the following: sample 476: $Alm_{77–79}Sps_{3–4}Grs_4Prp_{14–15}$; sample Eá–7: $Alm_{83–86}Sps_{4–8}Grs_{2–3}Prp_{5–10}$; and sample Szl–3: $Alm_{82–85}Sps_{4–8}Grs_{2–3}Prp_{7–10}$.

4.4. Phyllosilicate X-ray powder diffraction mineralogy

According to semiquantitative XRPD analysis (in mass%), the separated and phyllosilicate-rich part of the most deformed pyroclastic rock sample (matrix material, sample 177/1) has a bulk mineral composition with 40–50% quartz, 30–40% illite ± muscovite, and 10–20% albitic plagioclase with minor calcite. The modal compositions of the three clay (< 2 μm grain size) fraction specimens are rather similar to those of the matrix material and are predominated by illite ± muscovite and quartz, with minor albitic plagioclase and trace amounts of calcite.

The position of the 00,10 reflection of the phyllosilicates ranges between 1.986 and 1.990 Å *d* spacing ($n = 9$) which is lesser than that of the ideal muscovite (1.996 Å). Furthermore, a significant shoulder can be observed on the high angle side of this peak near 1.982 Å, suggesting a moderate substitution of Na or Ca referring to 'mixed' K-Na-mica (Livi et al., 1997). After ethylene glycol solvation of the specimens, illite ± muscovite did not show expandability. Consequently, it does not contain smectitic swelling phase as interstratification. The diagnostic *d* spacings of the illite ± muscovite (3.74 Å, 3.00 Å, and 2.80 Å) indicate that the investigated material is predominated by the $2M_1$ polytype.

The Esquevin indices of the illite ± muscovite (I(002) / I(001) ratio; Esquevin, 1969) are 0.19, 0.22, and 0.25 which denote a relatively Fe-rich composition (biotite + muscovite) for the studied material. The KI_{Basel} values of the three corresponding specimens are 0.223 ± 0.002, 0.226 ± 0.002, and 0.229 ± 0.002 $\Delta^\circ 2\Theta$, respectively, after triplicate analyses (Supplementary Fig. 5). The mean apparent crystallite size of mica calculated after the Scherrer equation (Klug and Alexander, 1974; Merriman et al., 1990) shows a value of 638 ± 11 Å ($n = 3$). Both the KI_{Basel} and crystallite size values refer to the epizone (Árkai et al., 1996).

4.5. Geochronology

4.5.1. Illite K-Ar ages

The K-Ar radioisotopic age data of the phyllosilicate-rich part of the most deformed pyroclastic rock (matrix material, sample 177/1) and those of the separated clay fractions slightly differ and yield ages 98.32 ± 1.40 Ma, 92.32 ± 1.31 Ma, and 80.3 ± 1.14 Ma, respectively (Table 2). These results indicate that the three samples are nearly cogenetic. Based on the results of the petrographic and XRPD examinations, only the illitic material ('mixed' K-Na-mica) is a relevant K-bearing mineral that is considered a product of a progressive metamorphic event.

4.5.2. Zircon textures and U-Pb ages

The studied zircons (some representative crystals displayed in Fig. 8) are 100–400 μm long, brownish gray crystals or fragments. Euhedral (bipyramidal or prismatic) and subhedral (variably resorbed) zircon crystals occur equally, and their shapes vary from relatively isometric to

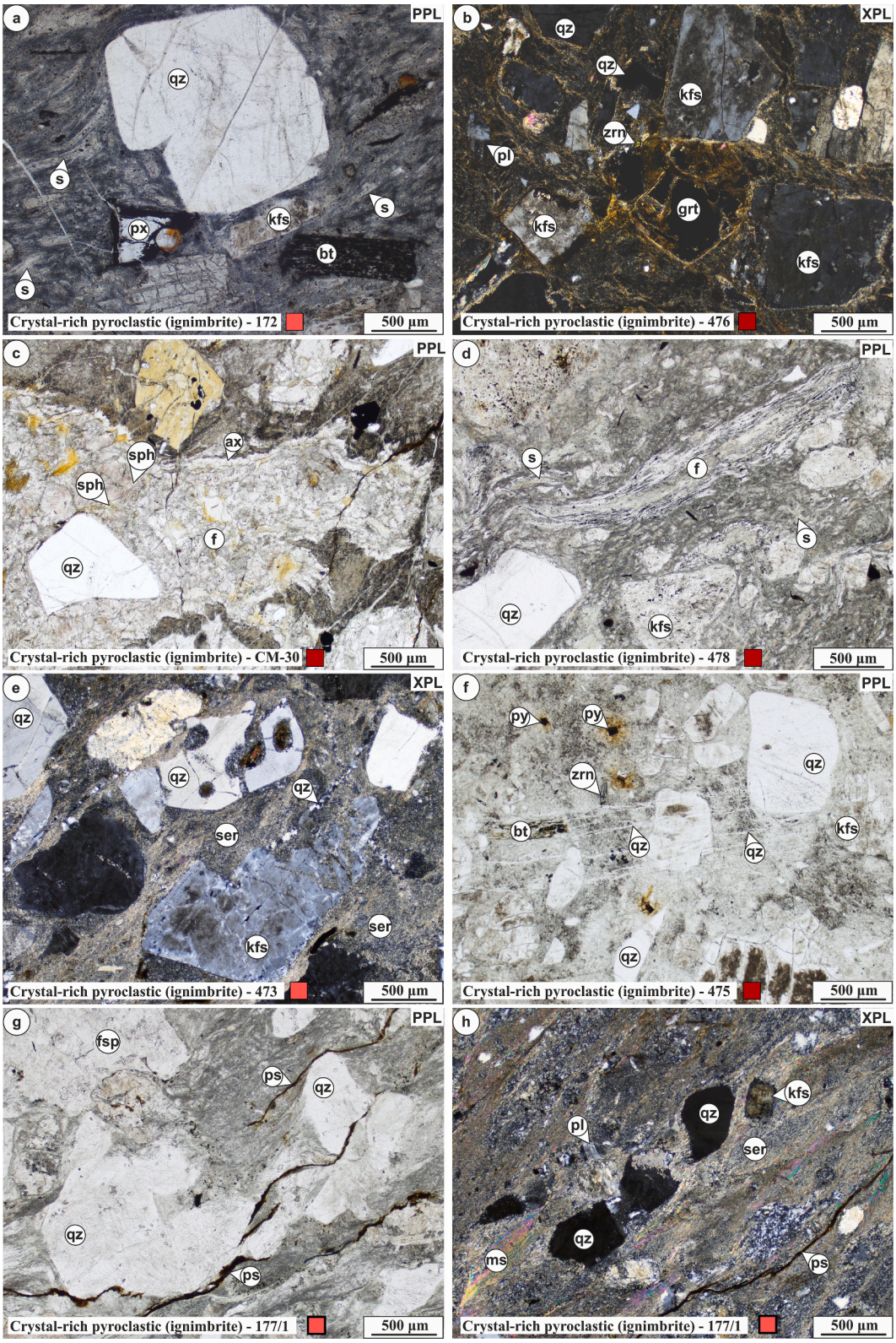

Fig. 2. Photomicrographs of some representative crystal-rich pyroclastic rocks (rhyodacitic/dacitic ignimbrites) in the Apuseni Mts. (a–d) variously welded, non-deformed ignimbrites with well-preserved pyroclastic texture (Codru-Moma and Bihor Mts); (e–f) sericitized, hydrothermally overprinted ignimbrites with secondary quartz and pyrite (Codru-Moma and Bihor Mts); (g–h) strongly altered and tectonically deformed ignimbrites with well-developed foliation (Bihor Mts). Abbreviations: *ax* axiolite, *bt* (pseudomorph after) biotite, *f* altered fiamme, *fsp* feldspar (altered), *grt* garnet, *kfs* K-feldspar, *ms* muscovite, *pl* plagioclase, *ps* pressure-solution seams, *px* (pseudomorph after) pyroxene, *py* pyrite, *qz* quartz, *s* altered glass shard, *ser* sericite, *sph* spherulite, *zrn* zircon, *PPL* plane polarized light, *XPL* crossed polars.

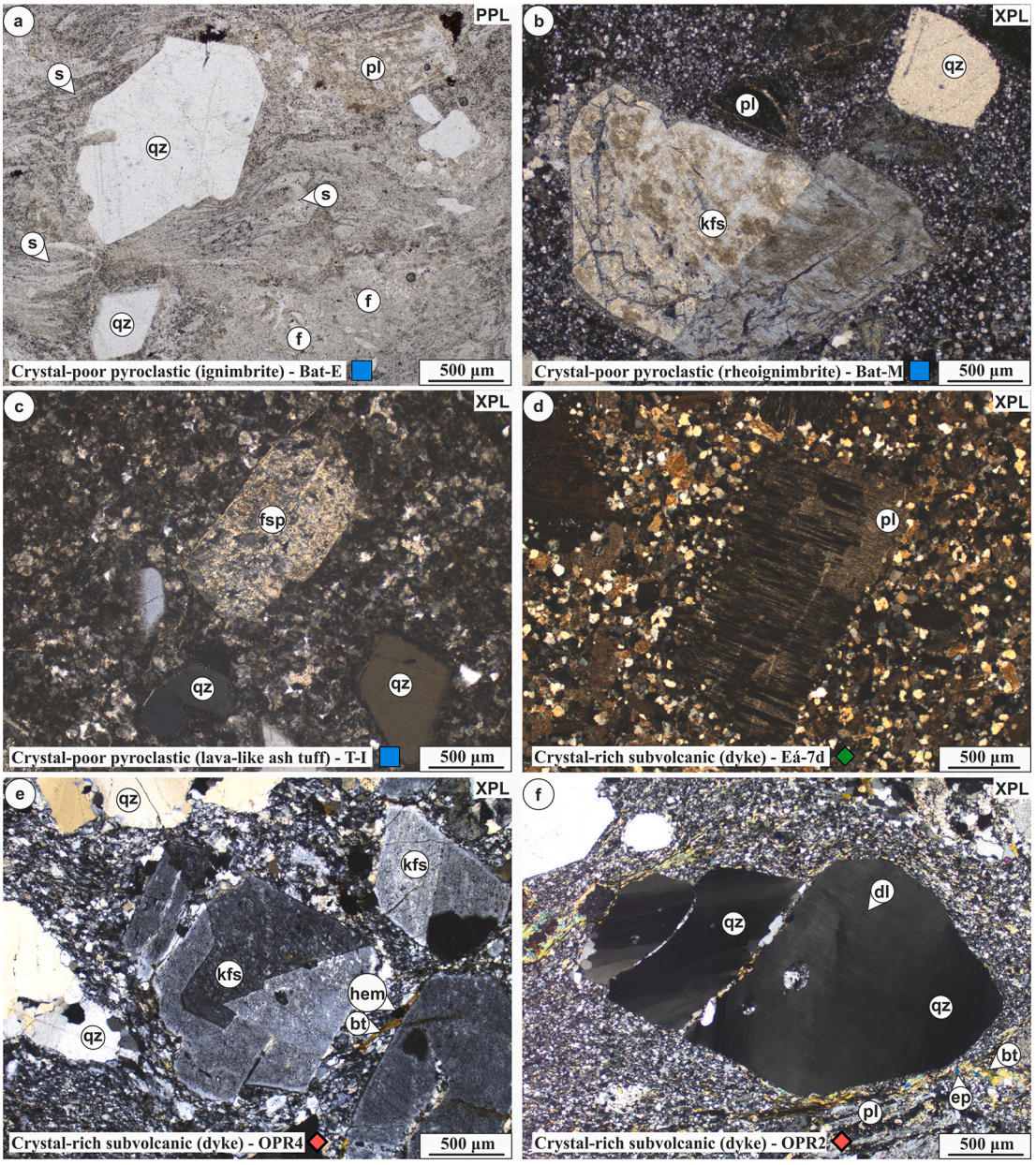

Fig. 3. Photomicrographs of some representative crystal-poor pyroclastic rocks (rhyolites) in the Battonya–Pusztaföldvár Basement Ridge (a–c), eastern Pannonian Basin (welded, rheomorphic ignimbrites, and lava-like ash tuffs, respectively); (d) rhyodacitic/dacitic dyke in southern Transdanubia; and (e–f) variously deformed rhyolitic dykes in the Highiş Mts (SW Apuseni Mts). Abbreviations: *bt* biotite, *dl* deformation lamellae, *ep* epidote, *f* altered fiamme, *fsp* feldspar (altered), *hem* hematite, *kfs* K-feldspar, *pl* plagioclase, *qr* quartz ribbons, *qz* quartz, *s* altered glass shard, *PPL* plane polarized light, *XPL* crossed polars.

strongly elongated (up to an elongation ratio of 1:7). All of them show weak cathodoluminescence intensity and oscillatory zoning typical for magmatic zircon crystals except for the OPR1 sample where the hydrothermally overprinted, deformed texture is the dominant one. Thirteen to sixty-one laser spots were analyzed per samples, placed mostly in the mantle part of the crystals, avoiding cracks, inclusions, or inherited cores (Fig. 8). The data were not considered if >5% discordance was detected (see detailed in the Electronic Supplementary Material 1). The remaining dates usually give large age ranges, suggesting the presence of older (antecrystic or xenocrystic) cores and/or possible Pb loss. For interpretation of the Late Paleozoic ages the $^{206}Pb/^{238}U$ data were used. They have an average 2 s uncertainty between 1.4 and 2.3%. The average Th/U ratios (0.2–0.9) as well as U concentrations within the samples usually do not give any systematic relation to the $^{206}Pb/^{238}U$ dates (Supplementary Fig. 6).

We calculated concordia ages (IsoplotR; Vermeesch, 2018), omitting discordant, older (antecrystic or xenocrystic), or significantly younger dates (possibly affected by Pb loss). Moreover, we used the $^{206}Pb/^{238}U$ dates to calculate low Mean Standard Weighted Deviation (MSWD) weighted mean ages considered to be the youngest population ages. The selected group of dates for each sample included the youngest dates (without younger outliers) to older dates until the MSWD remains below a threshold value indicating isochronous age (Wendt and Carl, 1991). Both the concordia and the weighted mean age calculations resulted similar, overlapping ages (Table 3) which we consider the closest to eruption event ages. The interpreted eruption ages are given by the youngest population ages and their uncertainties involving 1% external (systematic) error (Table 3).

4.5.3. Zircon age of crystal-rich (rhyodacitic/dacitic) pyroclastic rocks (Apuseni Mts and southern Transdanubia)

Zircon crystals from six samples (172, 476, 478, 479, CM-30, and

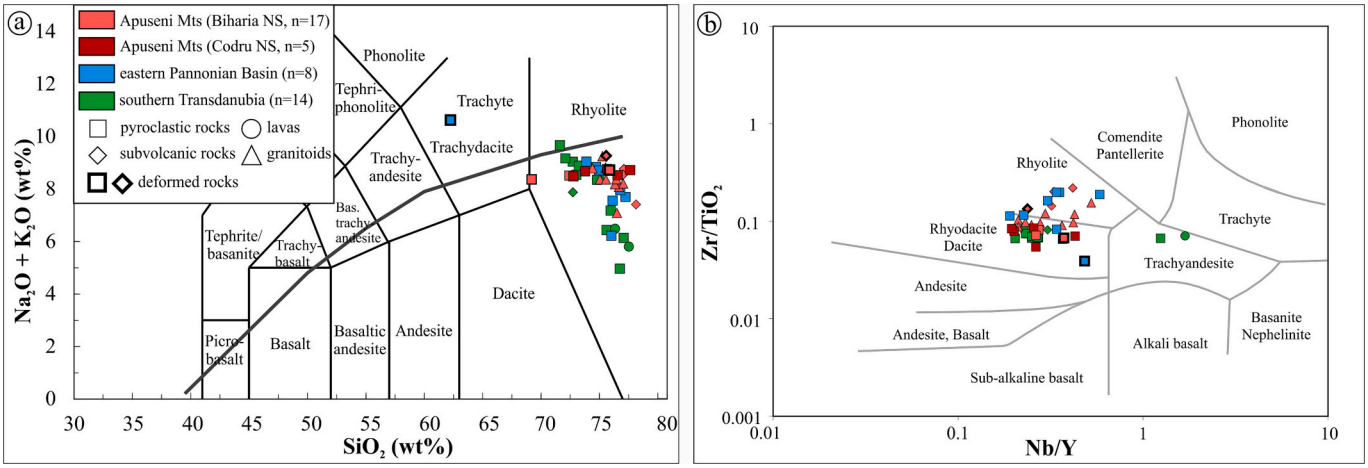

Fig. 4. Classification of the studied Permian felsic volcanic rocks (a) in the total alkali-silica (TAS) diagram (Le Maitre et al., 1989) and (b) the Zr/TiO_2 vs. Nb/Y diagram (Winchester and Floyd, 1977). Most of the studied volcanic rocks from the Pannonian Basin (Hungary) as well as the Permian Highiş granitoids (red triangles) were published in Szemerédi et al. (2020a) and Szemerédi et al. (2021), respectively. The number of the analyzed rock samples (n) that belong to each area (tectonic unit) is given in the brackets. (For interpretation of the references to colour in this figure legend, the reader is referred to the web version of this article.)

Bt–3) were analyzed (Fig. 9) that represent the group of weakly or nondeformed crystal-rich, rhyodacitic/dacitic pyroclastic rocks. Most of the analyses resulted concordant dates; however, 12–54% of the dates proved to be discordant. Some of the individual $^{206}Pb/^{238}U$ dates refer to inherited domains (from 556.7 ± 10.6 Ma to 279.6 ± 4.4 Ma), while a few younger dates (<260 Ma) might be the result of Pb loss. Youngest population age calculations (Table 3, Supplementary Fig. 7) yielded similar interpreted eruption ages from 270.4 ± 4.0 Ma to 266.6 ± 2.8 Ma (MSWD = 0.9–1.9, Table 3).

4.5.4. Zircon age of crystal-poor (rhyolitic) pyroclastic rocks (eastern Pannonian Basin)

Zircons from five samples (Bat–18, Bat-E, Bat-M, Nsz–2, and T–I) were analyzed (Fig. 10) that represent the relatively crystal-poor rhyolitic pyroclastic rocks of the eastern Pannonian Basin (Battonya–Pusztaföldvár BR). In this group, the frequency of discordant dates was generally higher, especially for samples derived from the most tectonized basement areas (Nsz–2 and T–I, 52% and 60%, respectively; Table 1, Pap, 1993; Szemerédi et al., 2020b). Some of the concordant dates are xenocrystic (2803.8 ± 34.1 Ma to 425.9 ± 6.4 Ma), and/or antecrystic (283.6 ± 4.8 Ma to 273.7 ± 3.9 Ma) or likely affected by Pb loss (<260 or 255 Ma). Interpreted eruption ages (Table 3, Supplementary Fig. 8) range between 268.6 ± 3.5 Ma and 260.2 ± 3.2 Ma, with MSWD values from 0.2 to 2.0.

4.5.5. Zircon age of felsic magmatic rocks having moderately to strongly deformed textures (Apuseni Mts and eastern Pannonian Basin, Kelebia area)

Three altered samples belong to this group (177/1, OPR1, and Kel–11, Fig. 11), two of which, the deformed pyroclastic rocks (177/1 and Kel–11), bear very similar textural features, therefore, described together in the following.

Zircon crystals from the two crystal-rich deformed ignimbrite samples yielded almost only concordant dates; however, in both samples, xenocrystic domains (650.9 ± 8.5 Ma to 295.4 ± 4.3 Ma) and/or antecrystic domains (281.3 ± 4.3 Ma to 277.3 ± 4.6 Ma) appear. Moreover, some younger (<260 Ma) dates could be affected by Pb loss. The interpreted eruption ages of these samples are 265.2 ± 3.1 Ma (177/1) and 263.0 ± 3.7 Ma (Kel–11), with MSWD values 1.7 and 2.3, respectively (Table 3, Supplementary Fig. 9).

In case of the strongly deformed subvolcanic OPR1 sample with hydrothermally overprinted zircon texture, 66% of the analyzed spots were found to be concordant and no xenocrystic or antecrystic cores were identified; however, two younger dates (<260 Ma) refer to possible Pb loss. The interpreted age of the OPR1 sample is 262.9 ± 2.8 Ma (MSWD = 1.5, Table 3, Supplementary Fig. 9).

5. Discussion

As the studied Permian magmatic rocks were affected by various types and degrees of postmagmatic alterations, their petrological, geochemical, and geochronological interpretations should not be carried out without the careful exploration of these modifications. Therefore, first, we discuss the alteration and deformation processes and their significance then the Permian magmatic systems as well as the stratigraphic concerns of the studied rocks, including local-to-regional correlations.

5.1. Petrological and geochemical significances

5.1.1. Pristine composition and alteration facies

In general, the mineralogical and chemical compositions of pyroclastic rocks such as welded ignimbrites can be modified by vapor-phase reactions and subsequent diagenetic processes (e.g., silicification, K- and/or Na-metasomatism). Furthermore, many ancient volcanic rocks were affected by various types and degrees of alterations, including recrystallization, hydrothermal overprint, and metamorphism (see, e.g., McPhie et al., 1993; Gifkins et al., 2005; Hübner et al., 2021). Previous studies (Bonin and Tatu, 2016; Nicolae et al., 2014; Szemerédi et al., 2020a, 2021; Tatu, 1998) revealed that the Permian felsic volcanic and plutonic rocks in the Tisza MU were also influenced by various postmagmatic alterations, including multiple hydrothermal effects and, locally, deformations (Alpine metamorphism, Miocene tectonics). Nicolae et al. (2014) highlighted that the Permian sequences in the Apuseni Mts are mainly located in the lower parts of the Alpine tectonic units, where the rocks were weakly to strongly deformed during the nappe stacking phase and the primary rock texture was often obliterated by foliation (Kounov and Schmid, 2013; Nicolae et al., 2014). Various degrees of mineralogical, textural, and microstructural modifications were observed in both the pyroclastic and felsic (sub)volcanic rocks studied (Figs. 2 and 3, Supplementary Figs. 1–3).

Regardless of their sampling sites, a wide range of mineral-scale alterations were observed in the studied rocks, the most common are sericitization, carbonatization, and albitization of feldspar, hematitization of biotite, and strong alteration of pyroxene (replaced by carbonate and opaque minerals) together with the devitrification of fiamme/pumices and the groundmass. In nondeformed samples, pervasive

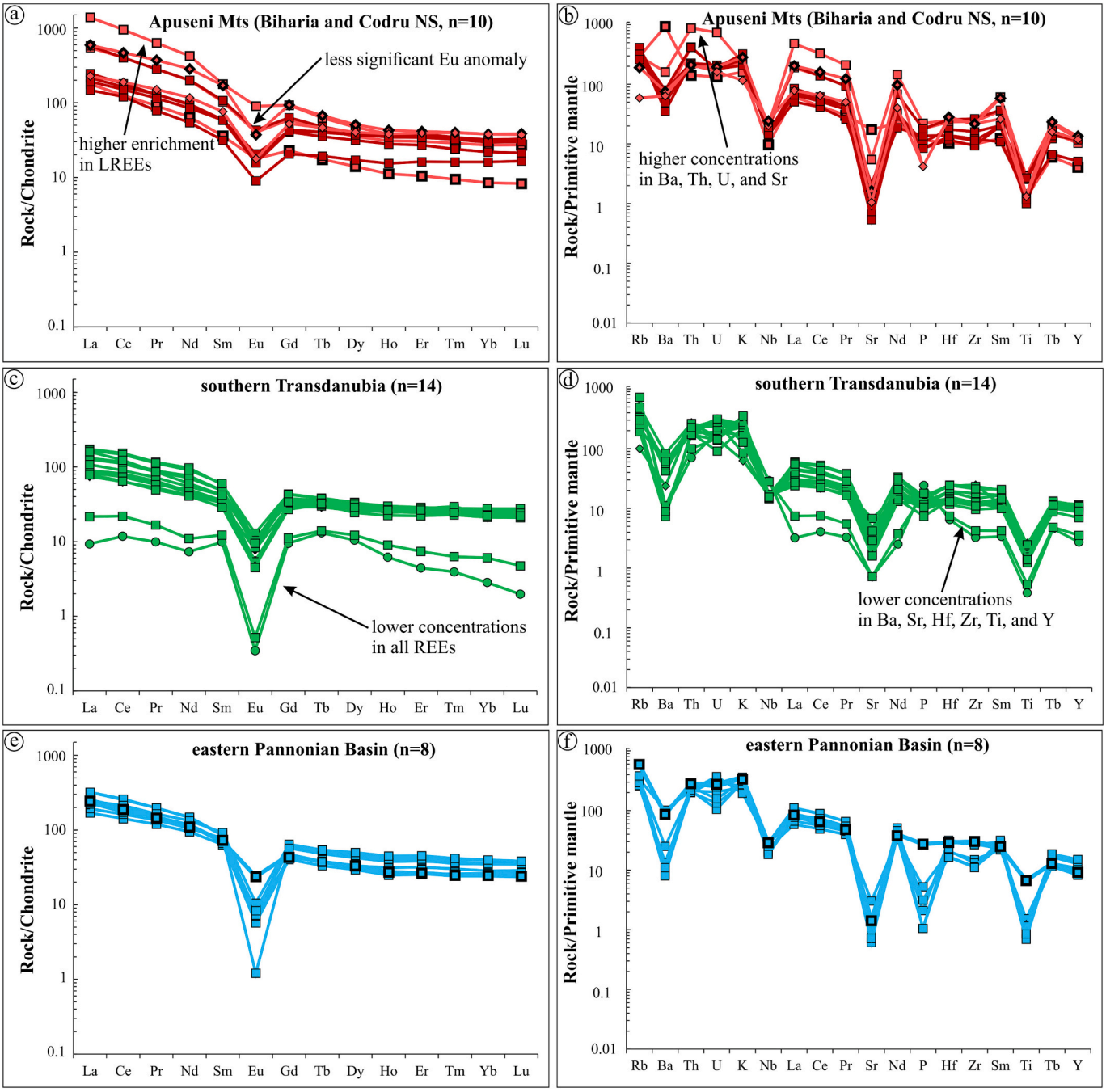

Fig. 5. Chondrite-normalized rare-earth element patterns (a, c, and e) and primitive mantle-normalized spider diagrams (b, d, and f) of the studied Permian felsic volcanic rocks (based on Sun and McDonough, 1989). Most of the studied volcanic rocks from the Pannonian Basin (Hungary) were published in Szemerédi et al. (2020a). The number of the analyzed rock samples (n) that belong to each area is given in the brackets.

silicification, sericitization, and thin veinlets could reflect external fluid-related processes. Furthermore, in the ductile deformed ignimbrites, strain shadows and fringe structures suggest that some minerals formed by direct precipitation from a mineralizing solution (Blenkinsop, 2000; Passchier and Trouw, 2005), potentially modifying the primary whole-rock compositions. The major chemistry with high LOI (8.20–8.64 wt %, Supplementary Tables 2 and 3), corresponding to the presence of secondary hydrous phyllosilicates and carbonates, can also support an open chemical system.

To verify the type and degree of alteration effects, some relevant ratios and indices of the major elements were calculated, revealing a wide range of alterations; however, granitoid rocks show the most pristine composition (Fig. 12). The Na_2O/Al_2O_3 vs. K_2O/Al_2O_3 and Na_2O/K_2O vs. SiO_2/Al_2O_3 diagrams (Figs. 12a and b) show that most of the samples, especially pyroclastic and lava rocks, lie outside the primary igneous field, reflecting a significant gain in K (up to 8.64 wt%, Supplementary Tables 2 and 3). The same trends were previously observed for the Permian felsic volcanic rocks of the Pannonian Basin, as well (Szemerédi et al., 2020a). Considering the alteration index (Ishikawa et al., 1976) and the Carbonate–Chlorite–Pyrite Index (Gifkins et al., 2005), as quantitative tools for measuring and discriminating the intensity of alteration (Shanks III and Thurston, 2012), the predominant process related to the studied rocks is hydrothermal sericitization (K-metasomatism), leading to higher values of K (Fig. 12c, Supplementary

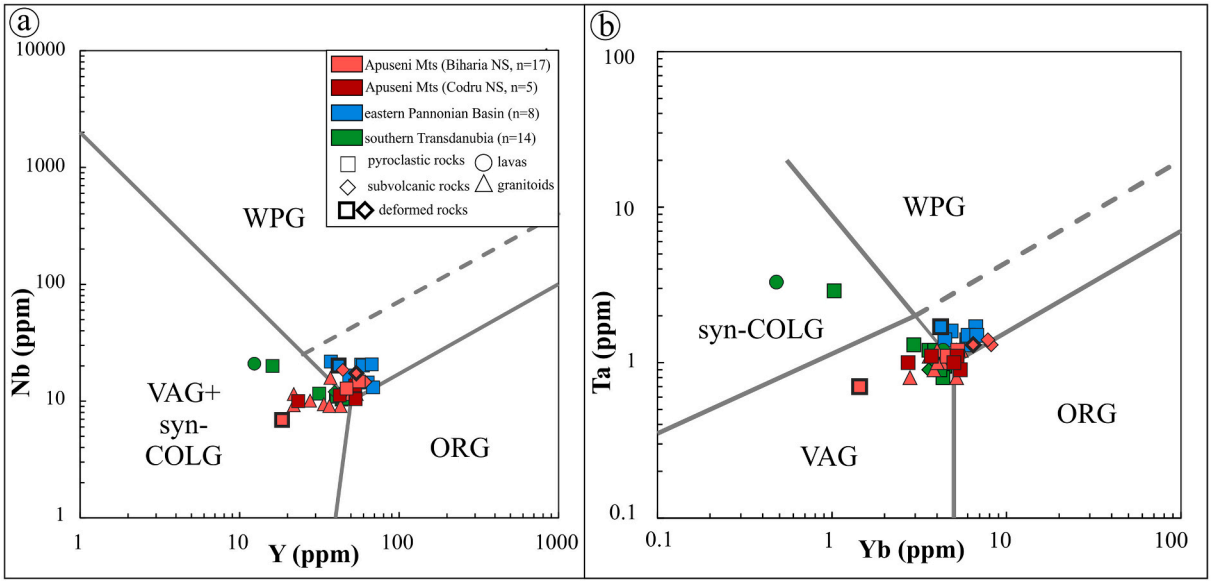

Fig. 6. (a) Y-Nb and (b) Yb-Ta diagrams (Pearce et al., 1984) for the geotectonic implications of the studied Permian felsic volcanic rocks. Most of the studied volcanic rocks from the Pannonian Basin (Hungary) as well as the Permian Highiş granitoids (red triangles) were published in Szemerédi et al. (2020a) and Szemerédi et al. (2021), respectively. The number of the analyzed rock samples (n) that belong to each area (tectonic unit) is given in the brackets. (For interpretation of the references to colour in this figure legend, the reader is referred to the web version of this article.)

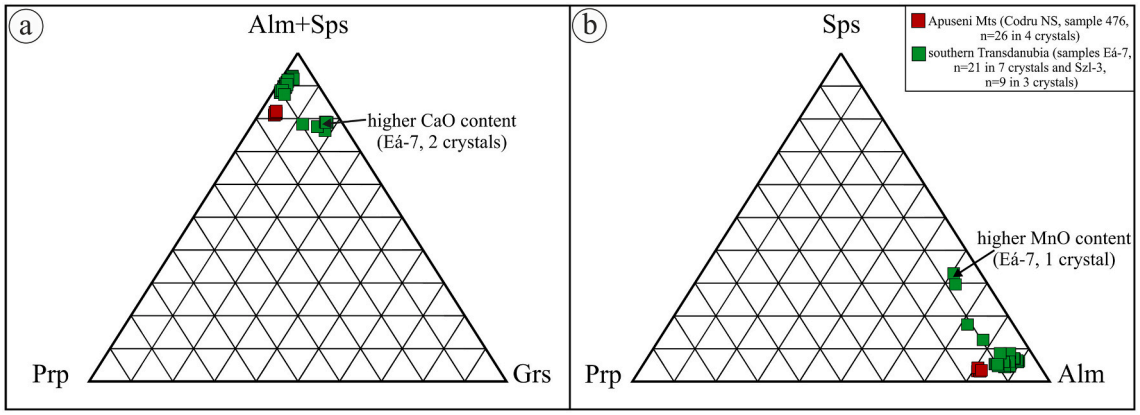

Fig. 7. Garnet compositions of the studied Permian felsic volcanic rocks (crystal-rich rhyodacitic/dacitic ignimbrites) from southern Transdanubia (northern foreland of the Villány Mts) and the Apuseni Mts (Codru-Moma Mts). Abbreviations: *Alm* almandine, *Grs* grossular, *Prp* pyrope, *Sps* spessartine. The number of the analyzed spots (n) and that of the garnet crystals belonging to each sample is given in the brackets.

Table 2
Results of the K-Ar analysis of the separated fractions of the sample 177/1 (strongly deformed crystal-rich pyroclastic rock).

Lab code	Sample type	Mineral	r $^{40}Ar^*/^{40}Ar_{tot}$	$^{40}Ar^*/m$ $\times10^{-6}$[ccSTP/g]	K (%)	Age (Ma)
9097	matrix material	Illite	0.66	10.21	2.600	98.32 ± 1.40
9097/A	<2 μm fraction	Illite	0.63	18.03	4.898	92.32 ± 1.31
9180	<1 μm fraction	Illite	0.69	12.11	3.797	80.21 ± 1.14
9180 (replicate)	<1 μm fraction	Illite	0.73	12.15	3.800	80.47 ± 1.14

Tables 2 and 3). Nevertheless, some diagenetic enrichment of K in the pyroclastic rocks and rare albitization of the Highiş aplite samples (Szemerédi et al., 2021) is also possible. It is important to note that the strongly deformed pyroclastic rock (sample 177/1) also plots in the least altered box, reflecting its alteration under nearly isochemical conditions. Nevertheless, the unaltered composition of the pyroclastic and volcanic rocks is difficult to determine; therefore, common diagrams for chemical classification and geotectonic discrimination using major elements or trace elements with similar geochemical behavior such as Rb (e.g., Pearce et al., 1984) are not applicable in a satisfactory manner.

On the other hand, the major element geochemistry of the Highiş granitoids and, most likely, of the related subvolcanic samples shows an unaltered, apparently primary magmatic composition (Fig. 12c). An anorogenic (A-type), continental rift-related character of the silicic magmas was previously suggested for these rocks, reflecting strong similarities with the aforementioned (sub)volcanic rocks (Bonin and

Fig. 8. Cathodoluminescence images of some representative zircon crystals from the samples Bt–3 (crystal-rich pyroclastic rock, southern Transdanubia), T–I (crystal-poor lava-like ash tuff, eastern Pannonian Basin), and 177/1 (deformed ignimbrite, Bihor Mts, Apuseni Mts). Spot IDs, concordant $^{206}Pb/^{238}U$ dates, and discordance values for the discordant dates are given in the figure, and the complete dataset is available in Electronic Supplementary Material 1. The length of the yellow scales beside each zircon crystal is 50 μm, while the diameter of the laser spots (red circles) is 33 μm. (For interpretation of the references to colour in this figure legend, the reader is referred to the web version of this article.)

Tatu, 2016; Szemerédi et al., 2020a, 2021; Tatu, 1998). Based on the Sr-Nd isotope geochemistry, Nicolae et al. (2014) argued for felsic magma generation within the lower crust because of the emplacement of mantle-derived mafic magmas that provided heat to partial melting, resulting a bimodal suite of volcanic rocks. The linear REE fractionation trend (Fig. 13) of the studied rocks further supports the common or similar source of the melts, showing increasing La_N and La_N/Yb_N values from crystal-rich samples (rhyodacites/dacites) towards relatively crystal-poor ones (rhyolites). The crystal-poor character of the eastern Pannonian samples, along with their generally higher HFSE and REE concentrations and slightly deeper negative Eu anomaly (Fig. 5, Supplementary Tables 2 and 3) indicate that they represent more fractionated melts than the crystal-rich samples of the Apuseni Mts and southern Transdanubia.

Among the various components, the garnet phenocrysts in some samples could also refer to the previously raised lower crustal conditions (Nicolae et al., 2014) and their composition (Fig. 7, Supplementary Table 4) could contain some petrogenetic information. In general, garnet, as a primary magmatic phase, can directly crystallize from hydrous melts with andesitic, dacitic, or rhyodacitic composition under high pressure and temperature conditions (9–18 kbar and 900–1000 °C, respectively; Green and Ringwood, 1968; Harangi et al., 2001; Alonso-Perez et al., 2009). Almandine-pyrope, as a high-pressure garnet variety, could further support the lower crustal origin of the felsic melts (see, e.g., Harangi et al., 2001). Unfortunately, however, the major elements in garnet, especially divalent cations (Fe, Mg, Ca, and Mn), diffuse sufficiently fast that their growth compositions are partially to completely modified in many petrologic systems (Devoir et al., 2021; Li et al., 2018). Clearly, the homogenized garnet composition within the studied crystals, without any zonation, could also reflect intracrystalline diffusive resetting.

Table 3
Compilation of the zircon in-situ geochronological results obtained on the studied Permian felsic volcanic rocks.

Area	Sample	Concordant[a]/all spots	Concordia age in Ma[b] with 2σ uncertainty (no. of analyses; MSWD)	Th/U range	Youngest population age[c] in Ma with 2σ uncertainty (no. of analyses; MSWD)	Eruption age with 2σ uncertainty (including external uncertainty[d])
Apuseni Mts	172 (cr, nd)	13/15	270.7 ± 2.1 (11; 1.6)	0.1–0.8	269.8 ± 1.7 (9; 1.9)	269.8 ± 3.2
	177/1 (cr, d)	22/25	266.1 ± 1.5 (18; 1.9)	0.1–1.8	265.2 ± 1.6 (15; 1.7)	265.2 ± 3.1
	476 (cr, nd)	11/15	267.9 ± 1.8 (11; 1.4)	0.3–1.2	267.3 ± 1.9 (10; 1.7)	267.3 ± 3.3
	478 (cr, nd)	11/13	268.5 ± 1.3 (10; 1.3)	0.1–0.4	268.4 ± 1.3 (10; 0.9)	268.4 ± 3.0
	479 (cr, nd)	46/61	266.9 ± 0.9 (43; 1.6)	0.1–1.2	266.6 ± 0.7 (41; 1.4)	266.6 ± 2.8
	CM-30 (cr, nd)	6/13	270.4 ± 2.9 (4; 1.0)	0.2–1.0	270.4 ± 2.9 (4; 1.0)	270.4 ± 4.0
	OPR1 (sv, d)	19/29	263.8 ± 1.7 (17; 3.7)	0.3–0.5	262.9 ± 1.0 (14; 1.5)	262.9 ± 2.8
Eastern Pannonian Basin	Bat–18 (cp, nd)	21/24	265.9 ± 1.3 (21; 2.5)	0.2–0.6	263.9 ± 1.0 (14; 1.7)	263.9 ± 2.8
	Bat-E (cp, nd)	18/28	265.4 ± 1.8 (16; 4.2)	0.2–0.4	262.9 ± 1.1 (10; 1.8)	262.9 ± 2.9
	Bat-M (cp, nd)	19/28	263.7 ± 1.5 (15; 2.2)	0.2–0.8	263.3 ± 1.0 (14; 1.7)	263.3 ± 2.8
	Nsz–2[#] (cp, d)	13/27	264.0 ± 2.4 (10; 3.2)	0.3–2.2	260.2 ± 1.9 (5; 0.2)	260.2 ± 3.2
	T–I[#] (cp, d)	10/25	268.4 ± 2.2 (8; 2.1)	0.2–0.5	268.6 ± 2.2 (8; 2.0)	268.6 ± 3.5
	Kel–11 (cr, d)	12/15	264.9 ± 2.9 (8; 3.7)	0.1–0.6	263.0 ± 2.6 (6; 2.3)	263.0 ± 3.7
Southern Transdanubia	Bt–3 (cr, nd)	22/25	268.3 ± 1.3 (19; 1.8)	0.2–1.3	268.4 ± 1.2 (19; 1.6)	268.4 ± 2.9

Th/U ratios are given for the concordant spots. Abbreviations: *cp* crystal-poor pyroclastic rock, *cr* crystal-rich pyroclastic rock, *sv* subvolcanic, *d* deformed, *nd* non-deformed.
[#]Samples from the most tectonized basement areas.
MSWD = Mean Standard Weighted Deviation.
[a] Concordant dates have discordance values <5% calculated as 100*(1-($^{206}Pb/^{238}U$ age)/($^{207}Pb/^{235}U$ age)).
[b] Concordia ages calculated by the IsoplotR software (Vermeesch, 2018) from concordant dates and without xenocrystic/antercrystic or possibly Pb loss affected dates.
[c] low MSWD weighted mean age considered to be the youngest population age: calculated from the $^{206}Pb/^{238}U$ dates of the sample including the youngest dates (without younger outliers) to older dates until the MSWD of weighted average remains below a threshold value indicating isochronous age (Wendt and Carl, 1991).
[d] propagated uncertainty is calculated by quadratic adding of uncertainty of ages and 1% external error of LA-ICP-MS measurements.

5.1.2. Conditions under dominant alteration and deformation events

Based on the petrographic and geochemical results (Fig. 12c), the predominant alteration of the studied rocks is a hydrothermal sericitization. Regarding the study area, several hydrothermal episodes should be considered; however, their roles cannot be quantitatively unraveled (Bonin and Tatu, 2016; Ciobanu et al., 2006; Fazekas and Vincze, 1991; Szemerédi et al., 2020a). Concerning the A-type Highiş granitoids, Bonin and Tatu (2016) suggested that the first hydrothermal episode (Na- and K-metasomatism caused by halogen-rich fluids on the massif scale) occurred by fluid exsolution shortly after the Guadalupian emplacement and during cooling. The complete subsolidus transformation of the rock-forming minerals was accompanied by greisen-type mineralization. It is possible that the apparently primary magmatic composition of the granitoid and subvolcanic samples, corresponding to the rhyolite field, reflects the result of that pervasive hydrothermal phase. Furthermore, Na-metasomatism (albitization) of aplite samples was closely related to this early process (Bonin and Tatu, 2016; Szemerédi et al., 2021) instead of 'diagenetic' modification.

Regarding the samples plotted in the hydrothermal sericitization field, their chemical composition could be variously overprinted by the Alpine tectonic events, which were accompanied by an influx of aqueous fluids and by mylonitization during greenschist to subgreenschist conditions (see, e.g., Árkai, 2001; Ciobanu et al., 2006; Kounov and Schmid, 2013; Bonin and Tatu, 2016). This process produced the alteration of K-feldspar to albite and sericite and led to the formation of white mica subparallel to the foliation in the deformed rocks. Additionally, some mineralization events that resulted in epidote-apatite-quartz veins were also related to this thermal episode (Ciobanu et al., 2006). Obviously, the slightly elevated concentrations of ΣREE, Y, Ce, and Th of some samples from the Apuseni Mts (Fig. 5a and b, Supplementary Tables 2 and 3) reflect the presence of secondary minerals such as epidote and biotite and support the influence of aqueous fluids channeled by brittle-ductile shear zones. Nevertheless, many of the studied samples, especially the nondeformed ones, were not affected by these compositional changes.

Regarding the reconstruction of physico-chemical conditions of ductile deformation, XRPD mineralogical data of the phyllosilicate-rich deformed ignimbrite sample (sample 177/1) yield additional information. The determined KI_{Basel} values and the mean apparent crystallite size of mica (0.223–0.229 and 638 ± 11 Å, respectively) prove that crystallization (i.e., ductile deformation) of the sericite-rich matrix progressed under conditions of greenschist facies (epizone; Árkai et al., 1996). This observation is confirmed by the presence of deformation lamellae in quartz porphyroclasts, also reflecting low-temperature conditions (300–400 °C; Blenkinsop, 2000; Passchier and Trouw, 2005). Additionally, the matrix forming white mica cannot be regarded as a relatively homogeneous substance, corresponding to the presence of 'mixed K-Na-mica' (Livi et al., 1997), which is a typical but metastable mineral under very low- and low-grade metamorphic conditions (Frey and Robinson, 1999). Based on micropetrographic observations (see Supplementary Figs. 2g and h), minor calcite is a ubiquitous component in the fine-grained matrix of the studied sample. This suggests that carbonatization could be related to the mineralizing solution during the ductile deformation. According to Mathieu (2018), when carbonate-

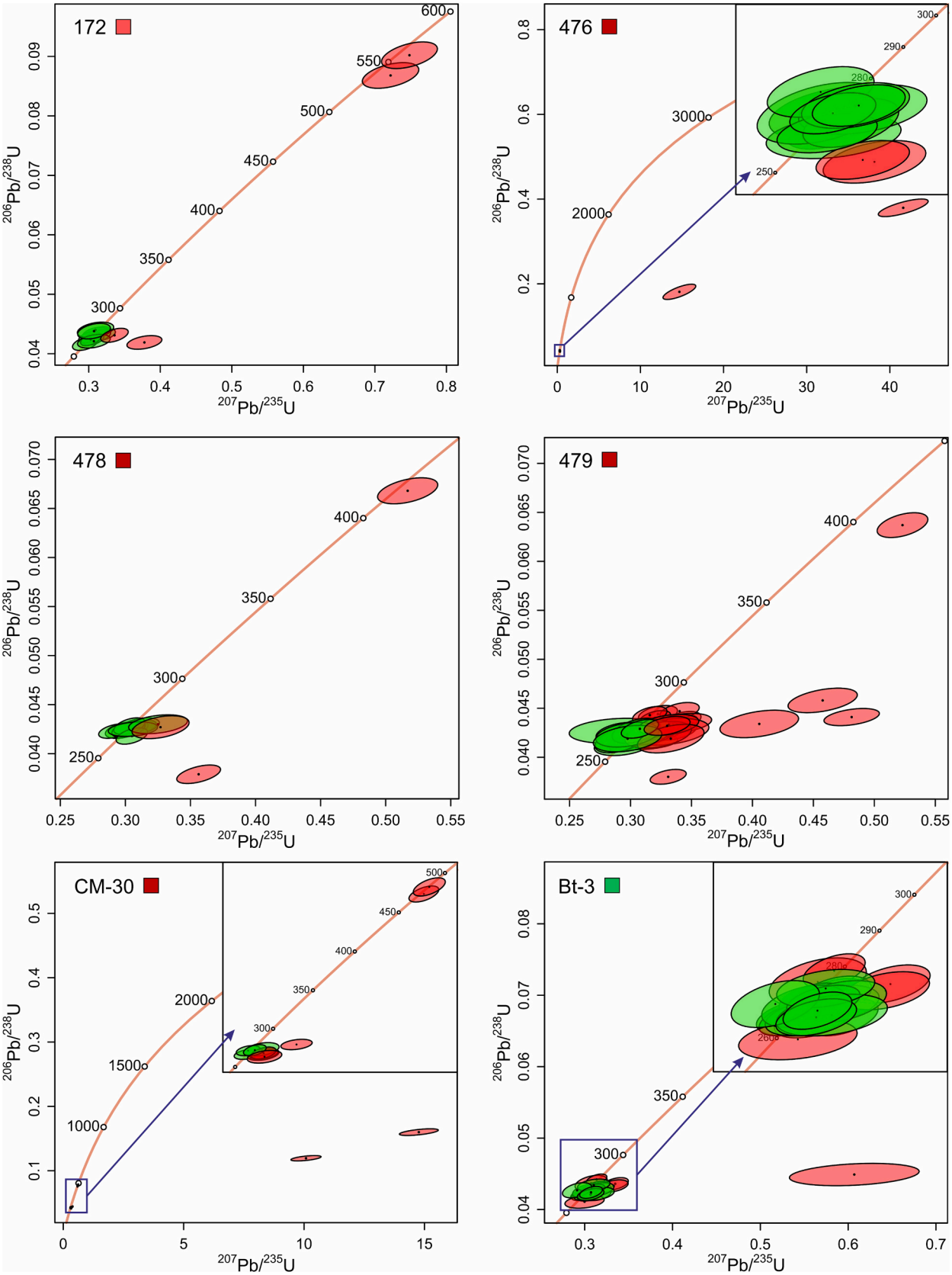

Fig. 9. Concordia age diagrams (Vermeesch, 2018) of the crystal-rich rhyodacitic/dacitic ignimbrites of the Apuseni Mts and southern Transdanubia. Green ellipses indicate concordant dates used for the concordia age calculations and the selection of the youngest coherent population of the $^{206}Pb/^{238}U$ dates to calculate low MSWD weighted means ages, while red ellipses indicate discordant, antecrystic/xenocrystic, or possible Pb loss affected dates. (For interpretation of the references to colour in this figure legend, the reader is referred to the web version of this article.)

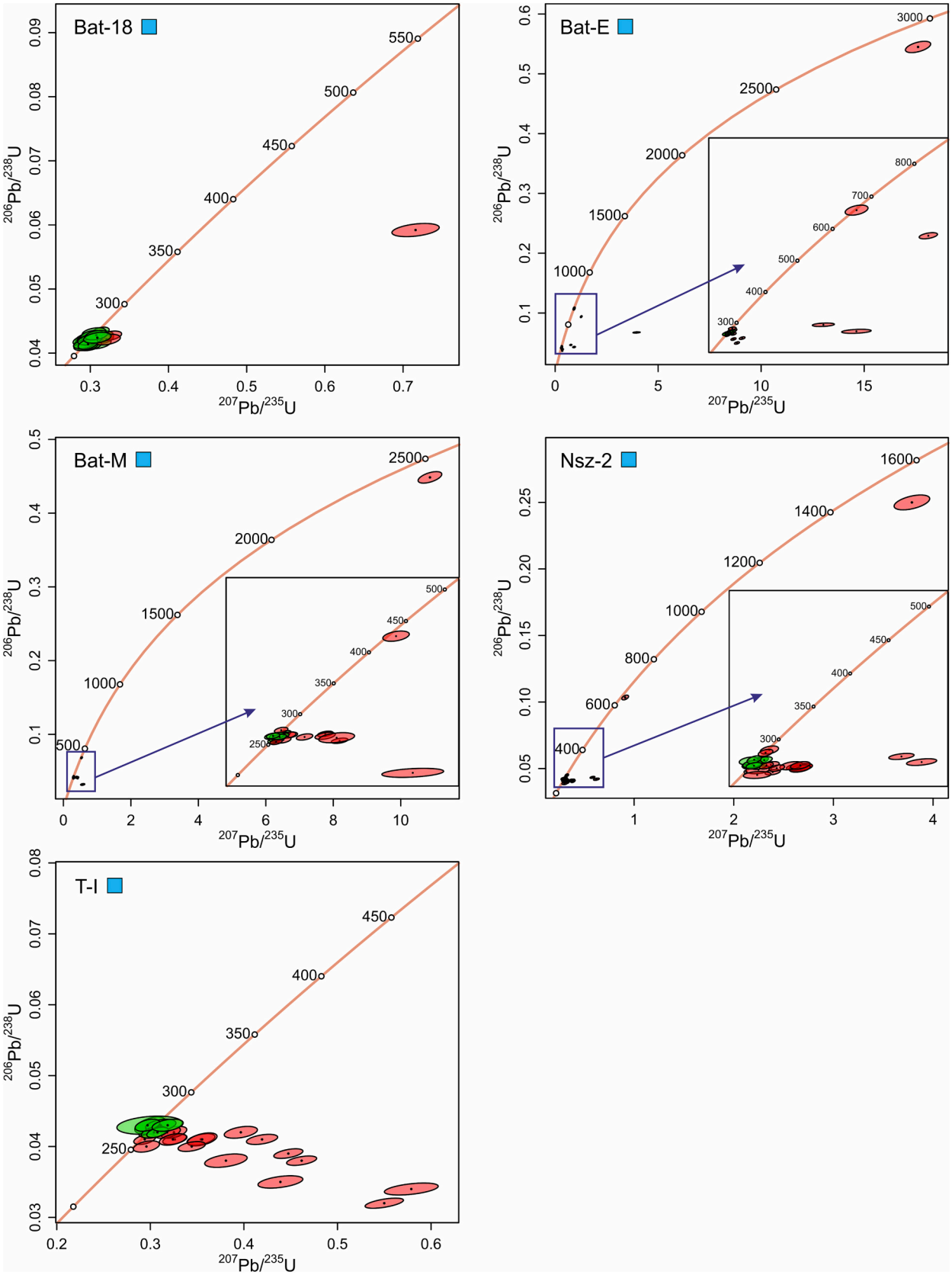

Fig. 10. Concordia age diagrams (Vermeesch, 2018) of the crystal-poor rhyolitic (rheo)ignimbrites and lava-like ash tuffs of the eastern Pannonian Basin. Green ellipses indicate concordant dates used for the concordia age calculations and the selection of the youngest coherent population of the $^{206}Pb/^{238}U$ dates to calculate low MSWD weighted means ages, while red ellipses indicate discordant, antecrystic/xenocrystic, or possible Pb loss affected dates. (For interpretation of the references to colour in this figure legend, the reader is referred to the web version of this article.)

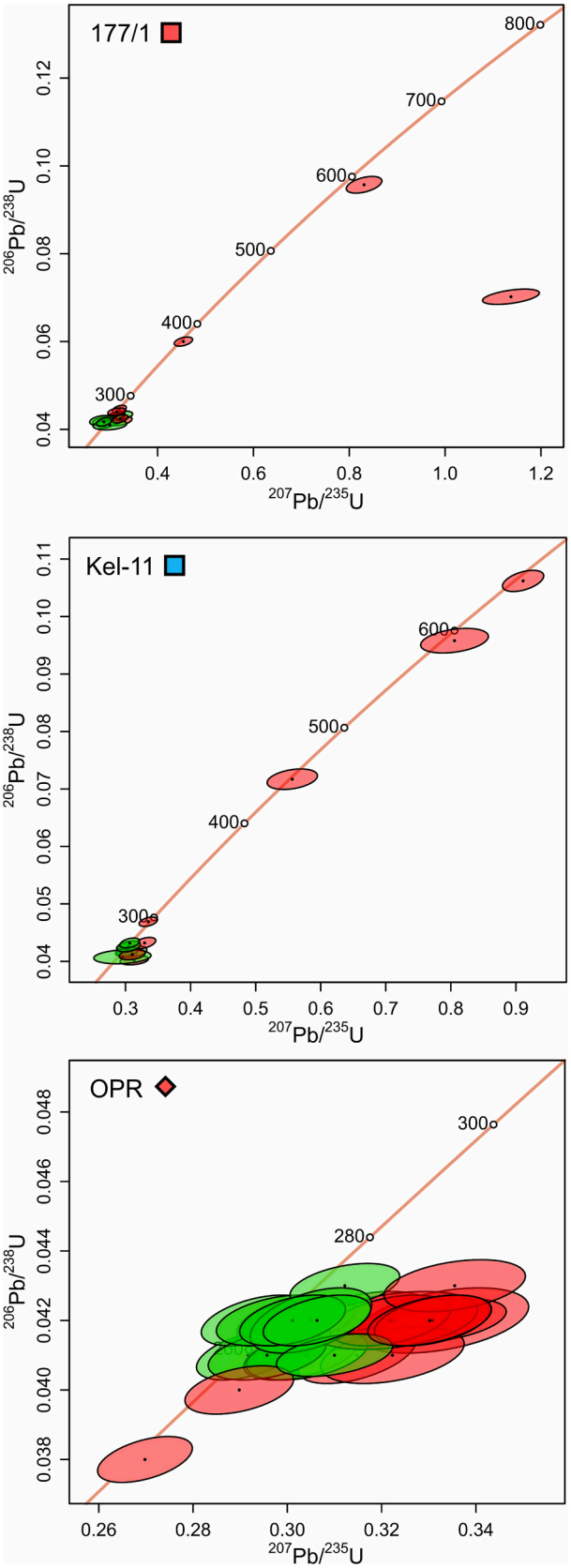

(caption on next column)

Fig. 11. Concordia age diagrams (Vermeesch, 2018) of the studied altered magmatic rocks, including deformed crystal-rich ignimbrites from the Bihor Mts (177/1) and the Kelebia area (Kel-11), and deformed, hydrothermally altered felsic subvolcanic rocks from the Highiş Mts (OPR1). Green ellipses indicate concordant dates used for the concordia age calculations and the selection of the youngest coherent population of the $^{206}Pb/^{238}U$ dates to calculate low MSWD weighted means ages, while red ellipses indicate discordant, antecrystic/xenocrystic, or possible Pb loss affected dates. (For interpretation of the references to colour in this figure legend, the reader is referred to the web version of this article.)

forming metasomatic alterations progress, carbon reacts with the calcium from plagioclase; therefore, albite, paragonite (sodium-rich white mica) and quartz form. More likely, the demonstrated semiquantitative mineralogical composition (i.e., quartz + albite + mixed K-Na-mica + calcite) can be interpreted as a result of the fluid-driven alteration during the ductile deformation.

The age of the deformation can be dated using the separated grain-size fractions of the illitic material (Table 2). Since the estimated maximum metamorphic temperature is higher than the closure temperature of the fine-grained white mica crystals (~260 °C; Hunziker, 1986; Hunziker et al., 1986), the relatively small difference of the K-Ar radioisotopic age data can be interpreted by the cooling age model, rather than the detrital effect. Considering that inherited illite grains tend to be enriched in the >2 μm grain-size fraction of mica-rich material from a deformed rock (see Clauer and Chaudhuri, 1999 and references therein), the age range of ~92–80 Ma obtained from the <2 μm fractions, probably predominated by newly formed or recrystallized illite, can be considered as the time of deformation of the measured sample. On the other hand, it cannot be excluded that the younger age could be caused by Ar loss. Therefore, the K-Ar data of the separated clay fractions reflect a Late Cretaceous (~98–80 Ma) metamorphism, indicating the effect of the main Alpine deformation (D2, Turonian nappe stacking, Kounov and Schmid, 2013) that forms the current geometry of the nappe stack in the Apuseni Mountains.

5.2. *Geochronological and stratigraphic significances*

5.2.1. *Permian magmatic systems*

In the Permian logs of the Apuseni Mts (see, e.g., Bleahu et al., 1981; Nicolae et al., 2014; Seghedi et al., 2001) felsic volcanic rocks were subdivided into two distinct levels: (1) a lower horizon (Early Permian, mainly rhyolitic ignimbrites and dykes) covered by mafic volcanics or sedimentary rocks and (2) an upper horizon as rhyolitic tuffs (Middle Permian without chronological data, sporadic bodies of ignimbrites, lava flows, and volcaniclastic rocks) intercalated with feldspathic sandstones, conglomerates, and shales. Following the sampling strategy of Nicolae et al. (2014), the studied ignimbrites collected in the Finiş, Dieva, Moma, Gârda, and Arieşeni Nappes (sensu Bleahu et al., 1981; Table 1) could represent the mentioned lower horizon, belonging to the Cisuralian formations proved by biostratigraphic data such as silicified wood remains and amphibian trace fossils within the intercalated sandstone beds (Seghedi et al., 2001; Nicolae et al., 2014).

However, subvolcanic OPR samples from the Highiş Mts unequivocally belong to the assumed upper rhyolitic level due to the intrusive emplacement of felsic A-type rocks, including porphyric microgranites, predated by the mafic igneous suite which is closely associated with the Lower Permian bioturbated siliciclastic rocks ("Vermiculate Sandstone Formation", also referred to as "Black Series" or Cladova Formation; Bordea and Bordea, 1993; Seghedi et al., 2001; Bonin and Tatu, 2016 and references therein). Furthermore, the Highiş granitoid rocks were dated by Pană et al. (2002, using the zircon U–Pb ID–TIMS method) and Szemerédi et al. (2021, using the zircon U–Pb LA–ICP–MS method), recording an igneous event of the Middle Permian (Guadalupian, 264 Ma and ~268–263 Ma, respectively).

Based on stratigraphic considerations, the Permian magmatism of

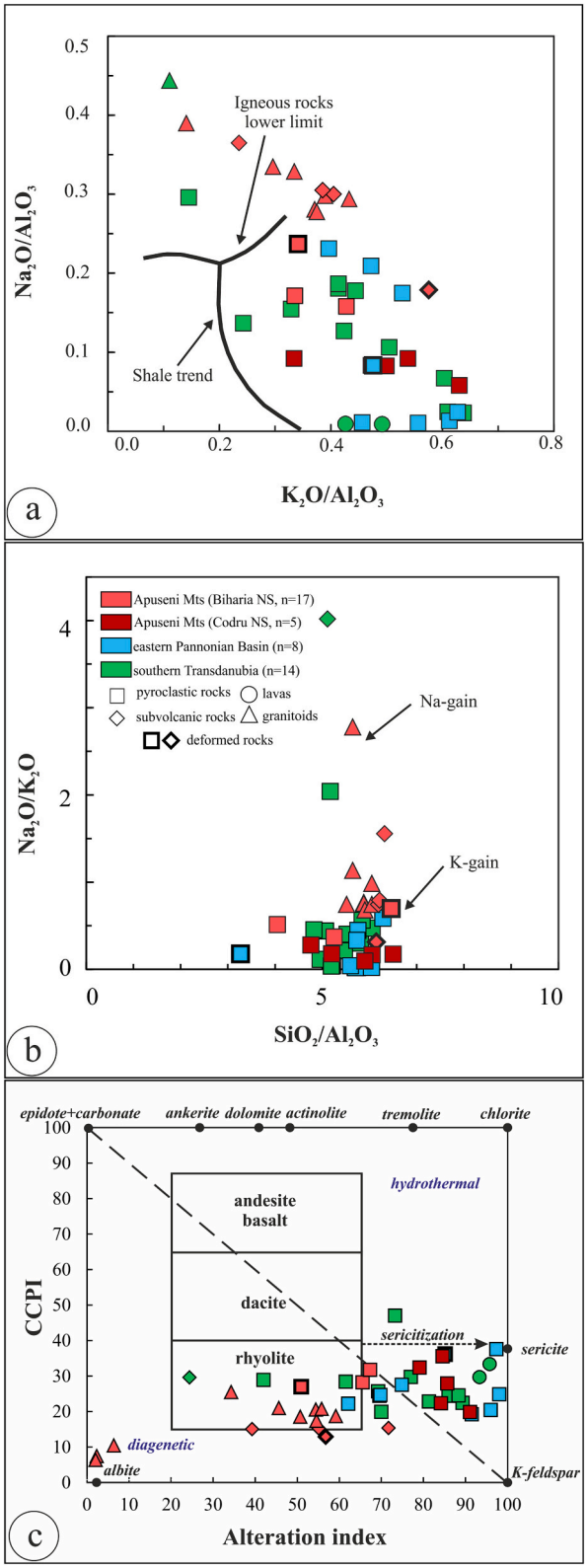

Fig. 12. (a) Na_2O/Al_2O_3 vs. K_2O/Al_2O_3 and (b) Na_2O/K_2O vs. SiO_2/Al_2O_3 diagrams (Garrels and Mackenzie, 1971), and (c) Alteration index (Ishikawa et al., 1976) vs. Carbonate–Chlorite–Pyrite Index (Gifkins et al., 2005) plot (modified after Shanks III and Thurston, 2012; Hübner et al., 2021) focusing on the postmagmatic alterations of the studied Permian volcanic rocks as well as the Highiş granitoids (Szemerédi et al., 2021).

the Hungarian part of the Tisza MU was traditionally regarded as the result of a single Cisuralian volcanic event (Barabásné Stuhl, 1988; Vozárová et al., 2009b). For the first time, zircon U-Pb concordia age data from the Battonya area (wells Battonya–32 and Battonya–53, eastern Pannonian Basin) were measured by Lelkes-Felvári and Klötzli (2010, published by Varga et al., 2015), placing the volcanism in the Early Permian (289.7 ± 6.2 Ma and 287.6 ± 7.2 Ma, respectively). A single sample of crystal-rich pyroclastic rock from southern Transdanubia (sample Gy–1, MkU) gave a younger weighted mean age of 271 ± 2.6 Ma (Varga et al., 2015, using the zircon U-Pb LA–ICP–MS method). According to the preliminary interpretation (Varga et al., 2015), however, the observed bimodal distribution of the concordant data (41 spots) could also suggest two distinct age populations, corresponding to an older volcanic episode and a younger one (33% and 67% of the concordant spots, 286.46 ± 0.82 and 267.96 ± 0.41 Ma, respectively; data were published by Szemerédi et al., 2020a). Recently, Szemerédi et al. (2020a) established that the Permian silicic volcanic rocks in southern Transdanubia and the eastern Pannonian Basin belong to the same Middle Permian (~267–260 Ma) continental rift-related magmatism. Except for the previously mentioned Gy–1 sample, slightly older (i.e., 290–275 Ma), most likely antecrystic domains were practically absent from the other studied samples (BATR/1, BATR/2, Kel–7, and Sz–1, see details in Szemerédi et al., 2020a).

Considering our new zircon ages and their uncertainties (Fig. 8 and Fig. 14, Table 3), interpreted age data strongly overlap without significant spatial differences. It should be noted, however, that the Alpine deformation rate is lost on concordant dates (for example, 265.2 ± 3.1 Ma for the strongly deformed sample 177/1 and 268.4 ± 2.9 Ma for the nondeformed sample Bt–3). Normal, magmatic Th/U ratios (Th/U > 0.1; Table 3) and the absence of characteristic metamorphic features (except for the OPR1 sample) such as grain size reduction, subgrain (domain) formation, irregular sectors, patchy or heterogeneous CL zoning, rim crystallization, and irregular, porous zircon overgrowths (see, e.g., Wayne and Sinha, 1988; Timms et al., 2006; Kirkland et al., 2009, 2015; Kaczmarek et al., 2011) suggest that the Cretaceous shearing event caused no observable disturbance in the U-Pb isotopic systematics of the zircons. Very likely, Alpine deformation processes were associated with relatively noncorrosive aqueous fluids, which dominantly formed hydrous phyllosilicates (hydrothermal sericitization) and carbonates under low-grade metamorphic conditions, as discussed above.

On the other hand, during the Alpine and, more probably, the subsequent Neogene tectonic episodes, especially in the basement of the eastern Pannonian Basin (Pap, 1993; Szemerédi et al., 2020b), the relatively high number of discordant dates for samples Nsz–2 and T–I (Fig. 10, Table 3, ESM 1) could reflect direct evidence of deformation-related modification of the U-Pb system in zircon (Pb loss and/or U gain). In tectonized zones during ductile and/or brittle deformation, low-temperature fluids can penetrate fractured zircons and preferentially leach radiogenic Pb out of the metamict grains (Wayne and Sinha, 1988).

Based on the presented geochronological results (Fig. 14, Table 3), it is not possible to distinguish two definite volcanic episodes and the associated stratigraphic levels. In general, referred to Scenario A, it can be concluded that any Permian silicic volcanic rocks in the Apuseni Mts as well as in southern Transdanubia and the eastern Pannonian Basin (including data from Szemerédi et al., 2020a) refer to a voluminous Middle Permian (274–257 Ma) magmatism. Similarly, mafic to felsic plutonic rocks in the Highiş massif (see, e.g., Tatu, 1998; Ciobanu et al., 2006;Bonin and Tatu, 2016; Szemerédi et al., 2021) as well as the Permian mafic–intermediate lavas in the Codru-Moma Mts (Codru NS, see, e.g., Nicolae et al., 2014) most probably belong to the same continental rift-related bimodal magmatism.

However, referred to Scenario B, an alternative explanation can also be provided. As discussed before, the Highiş granitoid and subvolcanic samples, showing an apparently primary magmatic composition (Fig. 12), suffered from a penetrative alteration effect of halogen-rich

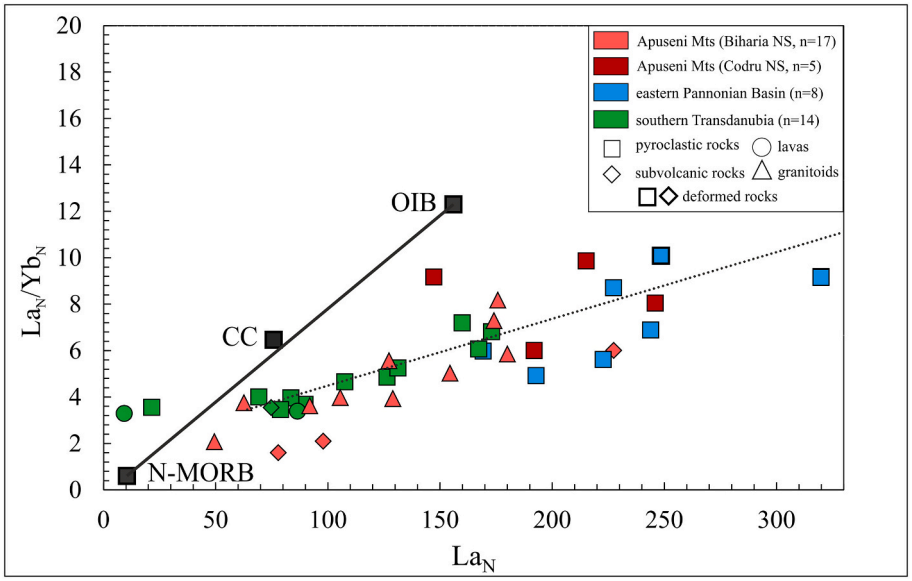

Fig. 13. La_N vs. La_N/Yb_N diagram of the studied Permian felsic volcanic rocks as well as the Highiş granitoids (SW Apuseni Mts). Note the linear positive trend suggesting fractional crystallization from a similar or common continental crustal source. Abbreviations: *CC* average continental crust (Rudnick and Gao, 2003), *N-MORB* Mid-Ocean Ridge Basalt (Sun and McDonough, 1989), *OIB* Ocean Island Basalt (Sun and McDonough, 1989).

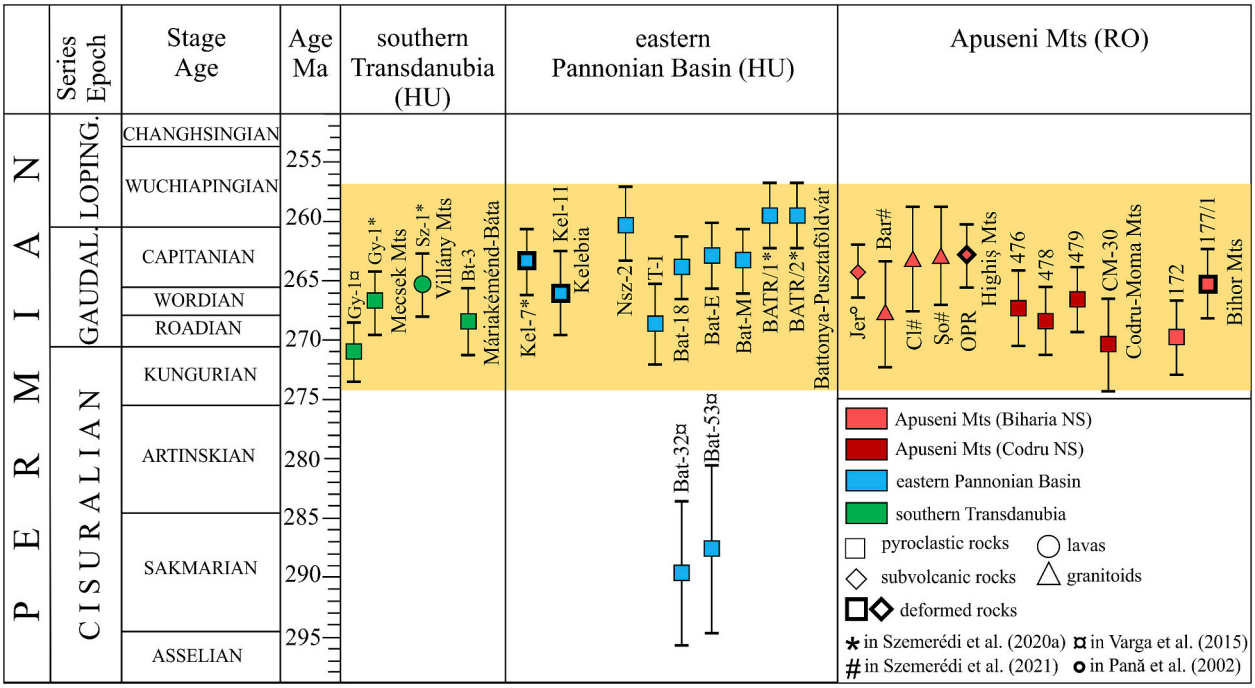

Fig. 14. Zircon U-Pb age data of the studied Permian felsic volcanic rocks (youngest population ages, condsidering 1% external errors), including previous results from the Pannonian Basin (Szemerédi et al., 2020a; Varga et al., 2015) as well as those of the Highiş granitoids (SW Apuseni Mts; Pană et al., 2002; Szemerédi et al., 2021).

fluids shortly after the Middle Permian emplacement (Bonin and Tatu, 2016; Szemerédi et al., 2021). In the case of the subvolcanic OPR1 sample, zircon crystals show a hydrothermally overprinted texture, so their early magmatic origin may be questioned. It is feasible that these zircons, which exclusively provide concordant dates, without antecrystic or xenocrystic cores are crystallized from a halogen-rich fluid that coexisted with the highly evolved residual magma during the magmatic–hydrothermal transition. Therefore, the zircon age of the OPR1 sample (262.9 ± 2.8 Ma) could represent the age of the halogen-rich fluid–melt interaction during the transition from magmatic to high-temperature hydrothermal stage of the Highiş pluton. Similar alterations are the most important factors that control the modification of highly evolved granitoid rocks and related mineralizations, and caution should be taken to interpret their isotopic data (see, e.g., Hoskin, 2005; Gusev, 2018; Zhi et al., 2021). Nevertheless, the widely used Th/U ratio, corresponding to a method to help distinguish metamorphic and magmatic zircons (Kirkland et al., 2015), and the age of this special type of hydrothermal zircon is often indistinguishable from magmatic zircon (Hoskin, 2005).

Obviously, the younger magmatic episode can be dated by the age of

the Highiş granitoid and subvolcanic samples (Guadalupian, ~268–263 Ma, Fig. 14). Based on trace element patterns (Figs. 4–6), zircon U-Pb ages (~269–260 Ma, Fig. 14) as well as Th/U ratios and U concentrations in their zircons (Supplementary Fig. 6), the crystal-poor ignimbrite samples from the eastern Pannonian Basin show strong similarities to those samples. However, with respect to the basement rocks, the relatively large age ranges, together with the negligible number of older cores, could suggest a possible loss of Pb during the later deformation episodes, resulting in far-traveled basement blocks with complex structure.

Characteristics of crystal-rich pyroclastic rocks of the Apuseni Mts and southern Transdanubia differ slightly in their trace element compositions (e.g., HFSE and REE concentrations) as well as in the Th/U ratios and U concentrations in their zircon crystals (Supplementary Fig. 6) and proved to be slightly older (~270–265 Ma, Fig. 14) than the crystal-poor rocks. Relatively large age ranges could also suggest a partial loss of Pb. Additionally, a rejuvenation caused by the possible hydrothermal effect of the later volcanic phase cannot be excluded. Nevertheless, the two proposed volcanic episodes cannot be distinguished from each other by the methods we used in this study in a satisfactory manner, and the presence of an Early Permian felsic magmatic phase remains unclear in the study area.

5.2.2. Stratigraphic concerns

The traditional subdivision of the study area (Fig. 1b to d) is based on its Mesozoic evolution, including three or four main Alpine nappe systems and several small nappes that have been defined according to stratigraphic and/or lithological principles and mainly without detailed tectonic studies (see, e.g., Bleahu et al., 1981; Balintoni, 1997;Nicolae et al., 2014; Seghedi et al., 2001). Therefore, divergent hypotheses and controversial nomenclature can be found in the regional literature (see, e.g., Schmid et al., 2008, 2020; Balintoni et al., 2009; Kounov and Schmid, 2013; Nicolae et al., 2014). As significant geochemical or geochronological differences were not identified among the studied felsic volcanic rocks, basically unique petrographic characteristics such as crystal-rich/poor development, garnet content, and type and degree of metamorphism could be used to improve local to regional correlations.

As mentioned above, the northern Apuseni Mts are traditionally subdivided into the Bihor NS, the Codru NS, and the Biharia NS from bottom to top. Within the sampling area, the Biharia NS are composed of three nappes that are the Arieşeni Nappe, the Gârda Nappe, and the Highiş–Muncel Nappe (Balintoni et al., 2009; Nicolae et al., 2014; Table 1). During the sampling, sample 473 was collected from the Arieşeni Nappe. According to Balintoni et al. (2002), however, the Arieşeni Nappe, which was the single unit of the Biharia NS involving both unmetamorphosed and metamorphosed Permian sequences, disappeared as an independent tectonic unit. Consequently, non-metamorphic Permian rocks have been attributed to Codru NS and mylonitized Permian rocks to the Biharia NS. Regarding the crystal-rich pyroclastic sample 473, the petrographic characteristics show intense hydrothermal alteration, but no indications of mylonitic deformation appear, reflecting that the sampling site corresponds to the Codru NS instead of the Biharia NS.

From a correlation point of view, the Permian samples derived from the Gârda Nappe (Biharia NS in the sense of Bleahu et al., 1981 and Nicolae et al., 2014) are also important. Crystal-rich, altered fiamme-bearing, and welded lapilli tuff (sample 172) shows well-preserved pyroclastic texture and its metamorphic overprint can be excluded. This indicates that the related sampling site could not belong to the Biharia NS. Furthermore, the mica-rich sample 177/1 suffered strong recrystallization and Turonian ductile deformation (~98–80 Ma; Table 2). This result fits well with the present-day tectonic sketch of the northern Apuseni Mts, since recently the Gârda Nappe is attributed to the Codru NS (Finiş–Gârda Nappe; Schmid et al., 2008; Kounov and Schmid, 2013; Reiser et al., 2017). According to Schmid et al. (2008), additionally, the pre-Triassic basement of the Gârda Unit in the Bihor Mts was ductile deformed in Turonian times. Similarly, Varga et al. (2023) highlighted that the Permo-Triassic cover succession, including Permian ignimbrites, was also affected by greenschist facies metamorphism and shearing in the Kelebia basement area (Békés–Codru NS, eastern Pannonian Basin).

On the other hand, Permian sequences are most abundant in the Codru NS, whereas they are only sporadic in the Bihor NS (Seghedi et al., 2001; Nicolae et al., 2014). Despite the volumetric differences compared to the Permian felsic volcanic rocks, the voluminous and chemically complex volcanic systems known in the northern foreland of the Villány Mountains and in the Máriakéménd–Báta area (Szemerédi et al., 2020a) are considered an integral part of the Hungarian continuation of the Bihor NS, belonging to the Villány–Bihor NS in southern Transdanubia (Csontos and Vörös, 2004; Fig. 1c and Table 1). However, the presence of garnet, with a very similar almandine composition, both in the crystal-rich ignimbrites of the northern foreland of the Villány Mts and in the Codru-Moma Mts (Finiş Nappe, Codru NS), suggests their common source. As garnet is absent in the felsic volcanic rocks of the Békés–Codru Unit, which are also crystal-poor in contrast to the rocks of the aforementioned areas, a close relationship can be proposed between the large-volume ignimbrites of Villány and Codru (instead of Bihor).

Finally, on a regional scale, the Permian magmatism in the Tisza Mega-unit proved to be significantly younger than similar episodes of the stable European plate (~300–290 Ma; e.g., Breitkreuz and Kennedy, 1999; Słodczyk et al., 2018). Similar, anorogenic, A-type geochemical features and zircon ages (~275–262 Ma) were documented from the crustal-scale superunits of the Western Carpathians (ALCAPA Mega-unit, A-type granitoids and/or silicic volcanic rocks of the Gemeric, Veporic, and Silicic Units) that could represent the closest analogies to the studied rocks in the Permian post-orogenic extension of the Paleo-Tethyan realm (e.g., Ondrejka et al., 2022; Villaseñor et al., 2021; Vozárová et al., 2009a).

6. Conclusions

Permian felsic volcanic rocks in the Tisza Mega-unit were affected by various postmagmatic alterations, including hydrothermal effects and/or deformation. Therefore, a complex study was conducted on pyroclastic and subvolcanic rocks collected from the Apuseni Mts (Romania) and the basement of the Pannonian Basin (Hungary), focusing not only on the Permian magmatism, but also on the various postmagmatic alterations and their significance in understanding regional processes and implying correlations. The following main results were obtained:

(1) Most of the studied volcanic rocks are crystal-rich and variously welded lapilli tuffs, showing a well-preserved pyroclastic texture. In contrast, the pyroclastic rocks of the Battonya–Pusztaföldvár Basement Ridge are relatively crystal-poor eutaxitic and rheomorphic lapilli tuffs, as well as lava-like ash tuffs. Felsic lavas and subvolcanic rocks are sporadic in the study area.
(2) The studied rocks belong to a Middle Permian (274–257 Ma) anorogenic tectonic setting (continental rift), and, unlike the previous assumptions, it is not possible to distinguish two definite volcanic episodes and the associated stratigraphic levels in the Permian sequences of the Tisza Mega-unit.
(3) Regardless of their sampling sites, a wide range of mineral-scale alterations were observed; the most common are the hydrothermal sericitization, carbonatization, albitization of feldspar, and hematitization of biotite. In nondeformed samples, pervasive silicification, sericitization, and thin veinlets could reflect external fluid-related processes.
(4) In tectonically deformed samples, hydrothermal sericitization was accompanied by mylonitization under conditions of greenschist to subgreenschist facies. K-Ar data of the separated clay fractions reflect a Late Cretaceous (~98–80 Ma) metamorphism,

indicating the effect of the main Alpine deformation in the Apuseni Mts.

(5) In the basement of the eastern Pannonian Basin, the relatively high number of discordant U-Pb dates could reflect evidence of deformation-related modification of the U-Pb system in zircon during the Alpine and, more likely, the subsequent Neogene tectonic episodes.

Petrographic features (e.g., crystal-richness/poorness or the presence/lack of garnet) of the studied felsic rocks, as well as the type and degree of metamorphism and deformation, were also applicable in the local correlations between the Alpine nappe systems in the Apuseni Mts and the analogous tectonic units in the basement of the Pannonian Basin.

Supplementary data to this article can be found online at https://doi.org/10.1016/j.lithos.2023.107330.

Declaration of Competing Interest

The authors declare that they have no known competing financial interests or personal relationships that could have appeared to influence the work reported in this paper.

Acknowledgements

Petrological, geochronological, and correlation studies were supported by the Hungarian National Research, Development and Innovation Office (projects K 131690 and K 108375) and also financed by the New National Excellence Program of the Ministry of Human Capacities (Hungary) to Máté Szemerédi (No. ÚNKP-18-3-I-SZTE-90 and ÚNKP-20-4-SZTE-596) and Andrea Varga (No. ÚNKP-18-4-SZTE-16). Additionally, this work was supported by the Bolyai Research Scholarship of the Hungarian Academy of Sciences (BO/266/18, Andrea Varga). Mihai Tatu and Ioan Seghedi were supported by Ministry of Research and Innovation, CNCS–UEFISCDI funding project PN-III-P4-ID-PCCF-2016-4-0014. We would like to thank Kristóf Fehér (MTA-ELTE Volcanology Research Group) for his help in SEM BSE and CL imaging. Furthermore, we are grateful to Andreas Kronz and Jochen Gätjen (Department of Geochemistry, University of Göttingen, Germany) for their assistance in the electron microprobe analyses of garnet crystals and to Csaba Vígh for his useful suggestions on garnet chemistry.

This paper is dedicated to the memory of our dear colleague, Mihai Tatu, who passed away while the manuscript was being reviewed.

References

Alonso-Perez, R., Müntener, O., Ulmer, P., 2009. Igneous garnet and amphibole fractionation in the roots of island arcs: experimental constraints on andesitic liquids. Contrib. Mineral. Petrol. 157, 541–558.

Árkai, P., 2001. Alpine regional metamorphism in the main tectonic units of Hungary: a review. Acta Geol. Hung. 44, 329–344.

Árkai, P., Merriman, R.J., Roberts, B., Peacor, P.R., Tóth, M., 1996. Crystallinity, crystallite size and lattice strain of illite-muscovite and chlorite: comparison of XRD and TEM data for diagenetic to epizonal pelites. Eur. J. Mineral. 8, 1119–1137.

Balintoni, I., 1997. Geotectonica terenurilor metamorfice din România. Ed. Carpatica, Cluj Napoca. Geotectonics of metamorphic terrains from Romania, Carpatica Publishouse (in Romanian).

Balintoni, I., Ghergari, L., Băbuţ, T., 2002. The Arieşeni Nappe, or the Moma and Poiana Nappes. Studia Universitatis Babeş-Bolyai, Geologia 47, 19–26.

Balintoni, I., Balica, C., Cliveţi, M., Li, L.Q., Hann, H.P., Chen, F., Schuller, V., 2009. The emplacement age of the Muntele Mare Variscan granite (Apuseni Mountains, Romania). Geol. Carpath. 60, 495–504.

Barabásné Stuhl, Á., 1988. A Dél-Baranyai dombság és a Villányi hegység permi képződményeinek kutatásáról készített összefoglaló jelentés IV. fejezete a permi képződményekről. Mecsekérc Ltd. (former Mecsek Ore Mining Company), pp. 100–213 (in Hungarian).

Bleahu, M., Lupu, M., Patrulius, D., Bordea, S., Stefan, A., Panin, S., 1981. The structure of the Apuseni Mountains. In: Guide to Excursion Book, 3. Bucharest, Association Carpatho-Balcanic Congress, XII.

Blenkinsop, T., 2000. Deformation Microstructures and Mechanisms in Minerals and Rocks. Kluwer Academic Publishers.

Bonin, B., Tatu, M., 2016. Cl-rich hydrous mafic mineral assemblages in the Highiş massif, Apuseni Mountains, Romania. Mineral. Petrol. 110, 447–469.

Bordea, S., Bordea, J., 1993. Presence of the "Vermiculate Sandstone Formation" (Permian) in the central zone of the Highiş Mts. Rom. J. Stratigr. 75, 17–19.

Breitkreuz, C., Kennedy, A., 1999. Magmatic flare-up at the Carboniferous/Permian boundary in the NE German Basin revealed by SHRIMP zircon ages. Tectonophysics 302, 307–326.

Ciobanu, C.L., Cook, N.J., Damian, F., Damian, G., 2006. Gold scavenged by bismuth melts: an example from Alpine shear-remobilizates in the Highiş Mts, Romania. Mineral. Petrol. 87, 351–384.

Clauer, N., Chaudhuri, S., 1999. Isotopic dating of very low-grade metasedimentary and metavolcanic rocks: Techniques and methods. In: Frey, M., Robinson, D. (Eds.), Low-Grade Metamorphism. Blackwell Science, Oxford, pp. 202–226.

Csontos, L., Vörös, A., 2004. Mesozoic plate tectonic reconstruction of the Carpathian region. Palaeogeogr. Palaeoclimatol. Palaeoecol. 210, 1–56.

Devoir, A., Bloch, E., Müntener, O., 2021. Residence time of igneous garnet in Si-rich magmatic systems: Insights from diffusion modeling of major and trace elements. Earth Planet. Sci. Lett. 560, 116771.

Esquevin, J., 1969. Influence de la composition chimique des illites sur leur cristallinité. Bulletin du Centre de Recherches Pau. SNPA 3, 147–153.

Fazekas, V., Vincze, J., 1991. Hidrotermás ércindikációk a Villányi-hegység északi előtere mélyfúrásaiban. Földtani Közlöny 121, 23–56 (in Hungarian).

Frey, M., Robinson, D., 1999. Low-Grade Metamorphism. Blackwell Science, Oxford.

Garrels, R.M., Mackenzie, F.T., 1971. Evolution of Sedimentary Rocks. Norton, New York.

Gifkins, C., Hermann, W., Large, R., 2005. Altered Volcanic Rocks: A Guide to Description and Interpretation. Centre for Ore Deposit Research, University of Tasmania, Australia.

Green, T.H., Ringwood, A.E., 1968. Origin of garnet phenocrysts in calc-alkaline rocks. Contrib. Mineral. Petrol. 18, 163–174.

Gusev, A.I., 2018. Composition of Magmatic and Hydrothermal Zircon in the Elinovskii Massif, Gorny Altai. Geol. Ore Deposits 60 (8), 708–716.

Harangi, Sz, Downes, H., Kósa, L., Szabó, Cs, Thirlwall, M.F., Mason, P.R.D., Mattey, D., 2001. Almandine Garnet in Calc-alkaline Volcanic Rocks of the Northern Pannonian Basin (Eastern–Central Europe): geochemistry, petrogenesis and geodynamic implications. J. Petrol. 42 (10), 1813–1843.

Horstwood, M.S.A., Košler, J., Gehrels, G., Jackson, S.E., McLean, N.M., Paton, C., Pearson, N.J., Sircombe, K., Sylvester, P., Vermeesch, P., Bowring, J.F., Condon, D.J., Schoene, B., 2016. Community-Derived Standards for LA-ICP-MS U-(Th)-Pb Geochronology – Uncertainity Propagation, Age Interpretation and Data Reporting. Geostand. Geoanal. Res. 40, 311–332.

Hoskin, P.W.O., 2005. Trace-element composition of hydrothermal zircon and the alteration of Hadean zircon from the Jack Hills, Australia. Geochim. Cosmochim. Acta 69, 637–648.

Hübner, M., Breitkreuz, C., Repstock, A., Schulz, B., Pietranik, A., Lapp, M., Heuer, F., 2021. Evolution of the lower Permian Rochlitz volcanic system, Eastern Germany: reconstruction of an intra-continental supereruption. Int. J. Earth Sci. 110, 1995–2020.

Hunziker, J.C., 1986. The evolution of illite to muscovite: an example of the behaviour of isotopes in low-grade metamorphic terrains. Chem. Geol. 57, 31–40.

Hunziker, J.C., Frey, M., Clauer, N., Dallmeyer, R.D., Friedrichsen, H., Flehmig, W., Hochstrasser, K., Roggwiler, P., Schwander, H., 1986. The evolution of illite to muscovite: mineralogical and isotopic data from the Glarus Alps, Switzerland. Contrib. Mineral. Petrol. 92, 157–180.

Ionescu, C., Hoeck, V., 2010. Mesozoic ophiolites and granitoids in the Apuseni Mountains. Acta Mineral.-Petrogr. Field Guide Ser. 20, 44.

Ishikawa, Y., Sawaguchi, T., Iwaya, S., Horiuchi, M., 1976. Delineation of prospecting targets for kuroko deposits based on modes of volcanism of underlying dacite and alteration Halos. Min. Geol. 26, 105–117.

Kaczmarek, M.-A., Reddy, S.M., Timms, N.E., 2011. Evolution of zircon deformation mechanism in a shear zone (Lanzo massif, Western-Alps). Lithos 127, 414–426.

Kirkland, C.L., Whitehouse, M.J., Slagstad, T., 2009. Fluid-assisted zircon and monazite growth within a shear zone: a case study from Finnmark, Arctic Norway. Contrib. Mineral. Petrol. 158, 637–657.

Kirkland, C.L., Smithies, R.H., Taylor, R.J.M., Evans, N., McDonald, B., 2015. Zircon Th/U ratios in magmatic environs. Lithos 212-215, 397–414.

Klug, H.E., Alexander, L.E., 1974. X-ray diffraction procedures for polycrystalline and amorphous materials. John Wiley and Sons, New York.

Kőrössy, L., 2005. Hydrocarbon geology of the southeastern Great Plain, Hungary. Part I. Általános Földtani Szemle 29, 41–132 (in Hungarian with English abstract).

Kounov, A., Schmid, S.M., 2013. Fission-track constraints on the thermal and tectonic evolution of the Apuseni Mountains (Romania). Int. J. Earth Sci. 102, 207–233.

Kübler, B., Jaboyedoff, M., 2000. Illite crystallinity. Earth Planet. Sci. Lett. 331, 75–89.

Le Maitre, R.W., Streckeisen, A., Zanettin, B., Le Bas, M.J., Bonin, B., Bateman, P., 1989. Igneous Rocks: A Classification and Glossary of Terms. Recommendations of the International Union of Geological Sciences Subcomission on the Systematics of Igneous Rocks. Blackwell, Oxford, pp. 1–256.

Li, B., Ge, J., Zhang, B., 2018. Diffusion in garnet: a review. Acta Geochimica 37, 19–31.

Livi, K.J.T., Veblen, D.R., Ferry, J.M., Frey, M., 1997. Evolution of 2:1 layered silicates in low-grade metamorphosed Liassic shales of Central Switzerland. J. Metamorph. Geol. 15, 323–344.

Mathieu, L., 2018. Quantifying hydrothermal alteration: a review of methods. Geosciences 8, 245.

Matsumoto, A., Kobayashi, T., 1995. K–Ar age determination of late Quaternary volcanic rocks using the "mass fractionation correction procedure": application to the Younger Ontake Volcano, central Japan. Chem. Geol. 125, 123–135.

McPhie, J., Doyle, M., Allen, R., 1993. Volcanic Textures: A Guide to the Interpretation of Textures in Volcanic Rocks. Centre for Ore Deposit and exploration Studies, University of Tasmania, Australia.
Merriman, R.J., Roberts, B., Peacor, D.R., 1990. A transmission electron microscope study of white mica crystallite size distribution in mudstone to slate transitional sequence, North Wales, UK. Contrib. Mineral. Petrol. 106, 27–40.
Nicolae, I., Seghedi, I., Boboş, I., Azevedo, M.R., Ribeiro, S., Tatu, M., 2014. Permian volcanic rocks from the Apuseni Mountains (Romania): geochemistry and tectonic constrains. Chem. Erde 74, 125–137.
Ondrejka, M., Vojtko, R., Putiš, M., Chew, D.M., Olšavský, M., Uher, P., Nemec, O., Drakou, F., Molnárová, A., Spišiak, J., 2022. Permian A-type rhyolites of the Drienok Nappe, Inner Western Carpathians, Slovakia: tectonic setting from in-situ zircon U–Pb LA-ICP-MS dating. Geol. Carpath. 73, 123–136.
Pană, D.I., Erdmer, P., 1994. Alpine crustal shear zones and pre-alpine basement terranes in the Romanian Carpathians and Apuseni Mountains. Geology 22, 807–810.
Pană, D.I., Heaman, L.M., Creaser, R.A., Erdmer, P., 2002. Pre-alpine crust in the Apuseni Mountains, Romania: insights from Sm-Nd and U-Pb data. J. Geol. 110, 341–354.
Pap, S., 1993. Subsurface geology of Fábiánsebestyén–Nagyszénás–Orosháza area. Földtani Közlöny 123, 69–98 (in Hungarian with English abstract).
Passchier, C.W., Trouw, R.A.J., 2005. Microtectonics. Springer-Verlag, Berlin, Heidelberg.
Pearce, J.A., Harris, N.B.W., Tindle, A.G., 1984. Trace element discrimination diagrams for the tectonic interpretation of granitic rocks. J. Petrol. 24, 956–983.
Reiser, M.K., Schuster, R., Spikings, R., Tropper, P., Fügenschuh, B., 2017. From nappe stacking to exhumation: cretaceous tectonics in the Apuseni Mountains (Romania). Int. J. Earth Sci. 106, 659–685.
Roduit, N., 2019. JMicroVision: Image Analysis Toolbox for Measuring and Quantifying Components of High-Definition Images. Version 1.3.1. https://jmicrovision.github.io.
Rudnick, R.L., Gao, S., 2003. Composition of the continental crust. Treatise Geochem. 3, 1–64.
Schmid, S.M., Bernoulli, D., Fügenschuh, B., Matenco, L., Schefer, S., Schuster, R., Tischler, M., Ustaszewski, K., 2008. The Alpine-Carpathian-Dinaridic orogenic system: correlation and evolution of tectonic units. Swiss J. Geosci. 101, 139–183.
Schmid, S.M., Fügenschuh, B., Kounov, A., Maţenco, L., Nievergelt, P., Oberhänsli, R., Pleuger, J., Schefer, S., Schuster, R., Tomljenović, B., Ustaszewski, K., van Hinsbergend, D.J.J., 2020. Tectonic units of the Alpine collision zone between Eastern Alps and western Turkey. Gondwana Res. 78, 308–374.
Seghedi, A., Popa, M., Oaie, G., Nicolae, I., 2001. The Permian system in Romania, Natura Bresciana. Ann. Mus. Civ. Sc. Nat. Monografia, Brescia 25, 281–293.
Shanks III, P.W.C., Thurston, R. (Eds.), 2012. Volcanogenic massive sulfide occurrence model: U.S. Geological Survey Scientific Investigations Report 2010–5070—C.
Słodczyk, E., Pietranik, A., Glynn, S., Wiedenbeck, M., Breitkreuz, C., Dhuime, B., 2018. Contrasting sources of Late Paleozoic rhyolite magma in the Polish Lowlands: evidence from U–Pb age and Hf and O isotope composition in zircon. Int. J. Earth Sci. 107, 2065.
Stampfli, G.M., Kozur, H.W., 2006. Europe from the Variscan to the Alpine cycles. In: Gee, D.G., Stephenson, R.A. (Eds.), European Lithosphere Dynamics, 32. Geological Society, London, pp. 57–82. Memoirs.
Sun, S.S., McDonough, W.F., 1989. Chemical and isotopic systematic of oceanic basalts implications for mantle compositions and processes. In: Saunders, A.D., Norry, M.J. (Eds.), Magmatism in Ocean Basins. 42. Geological Society London Special Publication, London, pp. 312–345.
Szederkényi, T., Haas, J., Nagymarosy, A., Hámor, G., 2013. Geology and history of evolution of the Tisza Mega-unit. In: Haas, J. (Ed.), Geology of Hungary, Regional Geology Reviews. Springer, pp. 103–148.
Szemerédi, M., Lukács, R., Varga, A., Dunkl, I., Józsa, S., Tatu, M., Pál-Molnár, E., Szepesi, J., Guillong, M., Szakmány, Gy, Harangi, Sz, 2020a. Permian felsic volcanic rocks in the Pannonian Basin (Hungary): new petrographic, geochemical and geochronological results. Int. J. Earth Sci. 109, 101–125.
Szemerédi, M., Varga, A., Szepesi, J., Pál-Molnár, E., Lukács, R., 2020b. Lavas or ignimbrites? Permian felsic volcanic rocks of the Tisza Mega-unit revisited: a petrographic study (SE Hungary). Cent. Eur. Geol. 63 (1), 1–18.
Szemerédi, M., Varga, A., Dunkl, I., Lukács, R., Seghedi, I., Kovács, Z., Raucsik, B., Pál-Molnár, E., 2021. Petrology and zircon U–Pb dating of granitoid rocks in the Highiş massif (SW Apuseni Mts, Romania): insights into Permian plutonic–volcanic connections. Geol. Carpath. 72, 482–504.
Tatu, M., 1998. Le Massif Highis (Roumanie), un exemple de l'évolution du magmatisme alcalin anorogénique. Ph D Thesis. Université Paris-Sud, Orsay.
Timms, N.E., Kinny, P.D., Reddy, S.M., 2006. Enhanced diffusion of Uranium and Thorium linked to crystal plasticity in zircon. Geochem. Trans. 7, 10.
Varga, A., Pál-Molnár, E., Raucsik, B., Schubert, F., Garaguly, I., Lukács, R., Kiss, B., 2015. Permian and Mesozoic formations of the S Great Hungarian Plain: integrating petrographic and geochemical results in tracking diagenetic history and regional relationship. In: Dályai, V., Sámson, M. (Eds.), Tisia Conference, Pécs, pp. 17–20 (in Hungarian).
Varga, A., Pál-Molnár, E., Raucsik, B., 2023. Revealing the mineralogical and petrographic signs of fluid-related processes in the Kelebia Basement Area (Szeged Basin, S Hungary): a case study of alpine prograde metamorphism in a permo-triassic succession. Geofluids 2023, 8600576.
Vermeesch, P., 2018. IsoplotR: a free and open toolbox for geochronology. Geosci. Front. 9, 1479–1493.
Villaseñor, G., Catlos, E.J., Broska, I., Kohút, M., Hraško, Ľ., Aguilera, K., Etzel, T.M., Kyle, J.R., Stockli, D.F., 2021. Evidence for widespread mid-Permian magmatic activity related to rifting following the Variscan orogeny (Western Carpathians). Lithos 390-391, 106083.
Vozárová, A., Šmelko, M., Paderin, I., 2009a. Permian single crystal U-Pb age of the Rožňava Formation volcanites (Southern Gemeric Unit, Western Carpathians, Slovakia). Geol. Carpath. 60, 439–448.
Vozárová, A., Ebner, F., Kovács, S., Kräutner, H.-G., Szederkényi, T., Krstić, B., Sremac, J., Aljinović, D., Novak, M., Skaberne, D., 2009b. Late Variscan (Carboniferous to Permian) environments in the Circum Pannonian Region. Geol. Carpath. 60, 71–104.
Warr, L.N., Mählmann, R.F., 2015. Recommendations for Kübler Index standardization. Clay Miner. 50, 282–285.
Wayne, D.M., Sinha, A.K., 1988. Physical and chemical response of zircons to deformation. Contrib. Mineral. Petrol. 98, 109–121.
Wendt, I., Carl, C., 1991. The statistical distribution of the mean squared weighted deviation. Chem. Geol. Isot. Geosci. Sect. 86, 275–285.
Winchester, J.A., Floyd, P.A., 1977. Geochemical discrimination of different magma series and their differentiation products using immobile elements. Chem. Geol. 20, 325–343.
Zhi, J., Lei, R., Chen, B., Muhtar, M.N., Feng, Z., Zhang, K., Cai, Y., Wu, C., 2021. Zircon genesis and geochronology for the zhangbaoshan super-large rubidium deposit in the Eastern Tianshan, NW China: implication to magmatic–hydrothermal evolution and mineralization processes. Front. Earth Sci. 9, 682720.